UNIVERSITY OF CALIFORNIA

Santa Barbara

# An investigation into the molecular mechanisms controlling neural tube closure in the basal chordate *Ciona*

A dissertation submitted in partial satisfaction of the requirements for the degree

Doctor of Philosophy in Molecular, Cellular, and Developmental Biology

by

Haley M. Smith

Committee in charge:

Professor William C. Smith, Chair

Professor Kathy R. Foltz

Professor Joel H. Rothman

Professor Anthony W. De Tomaso

December 2021

The dissertation of Haley M. Smith is approved.

_____

Kathy R. Foltz

_____

Joel H. Rothman

_____

Anthony W. De Tomaso

_____

William C. Smith, Committee Chair

December 2021

ACKOWLEDGEMENTS

There are many people who I owe a great amount of gratitude towards for helping me along the way in my graduate career. I will name a few of them here but know that there are many more who were also a part of my success.

I first must thank the many members of the Smith lab who I have had the pleasure to work alongside. They have been supportive, encouraging, and enjoyable colleagues. Matt and Erin have been a constant source of expert knowledge and willing to answer any of my questions. Steph, Cez, and Sam among others have been great friends. Our many great (and long) conversations about every topic under the sun helped to pass the time during long experiments. I thank Bill for the opportunity to work in his lab and for his support both in research and in pursuing many teaching opportunities that have brought me closer to my goals.

Graduate school certainly has its ups and downs, at times pushing you past your limits, but I will always be grateful for this journey because it has brought me friendships that will last a lifetime. Bridget, Christine, Claire, Anetka, and Priscilla, you have been the best housemates, cheerleaders, gym-buddies, supporters, and friends that are more like family. These are the people that I would absolutely not have made it through the finish line without.

I would also like to thank my family for their constant love and support in my life including my mom, dad, grandparents, Steve, Connor, and Nicole. Through many visits and phone calls they have encouraged me, cheered for me, and let me know they are proud of me regardless of my accomplishments. They have always shown great interest in what I do, even at times when they do not understand it.

Lastly, I would not be here without the sovereign hand of God in my life. Through the hills and the valleys, he has sustained me and led me to this point. Therefore, I must give the glory to whom it is due. Soli Deo gloria.

VITA OF HALEY M. SMITH

December 2021

---

EDUCATION

**University of California, Santa Barbara**
Doctor of Philosophy in Molecular, Cellular, and Developmental Biology, 2021
Certificate in College and University Teaching (CCUT), 2021

**Pepperdine University**
Bachelor of Science in Biology, 2015

---

WORK EXPERIENCE

**Pepperdine University (2021-2022)**
*Adjunct Faculty*
The Biochemical Basis of Human Disease (Fall 2021)

**University of California, Santa Barbara (2015-2021)**
*Teaching Associate*
Introductory Biology – Biochemistry, Cell Biology, & Genetics (Summer 2021)
Recombinant DNA Lab (Spring 2020)

*Teaching Assistant*
Biology Mentoring and Engagement I (Fall 2021)
Recombinant DNA Lab (Spring 2017, 2018, 2019, 2021)
Developmental Biology (Winter 2021)
Introductory Biology Lab (Fall 2015)

---

PUBLICATIONS & PRESENTATIONS

**Smith, H.M**., Khairallah, S.M., Nguyen, A.H., Newman-Smith, E., and Smith, W.C. (2021). Misregulation of cell adhesion molecules in the Ciona neural tube closure mutant bugeye. Dev. Biol. *480*, 14–24.

10th International Tunicate Meeting – Villefranche-sur-mer, France (7/2019)
West Coast Developmental Biology Regional Meeting – Cambria, CA (2/2019)
Society of Developmental Biology Annual Meeting – Portland, OR (7/2018)
Neuroscience Research Symposium – UCSB (5/2019) – Best Poster in Developmental Biology Award

ABSTRACT

An investigation into the molecular mechanisms controlling neural tube closure in the basal chordate *Ciona*

by

Haley M. Smith

Neural tube closure (NTC) is a fundamental process in the development of all chordates. During NTC, the developing central nervous system is transformed from a flat sheet of neural precursor cells into a hollow neural tube, which is the basic form that persists into the mature central nervous system. When the neural tube fails to properly close, neural tube defects (NTDs) result. NTDs are the most prevalent category of human birth defects, and they occur in about 1 out of every 1000 births. Previously, we discovered a NTC mutant (named *bugeye*) in the basal chordate *Ciona savignyi* that results from a defect in the gene encoding a T-Type Calcium Channel (Cav3). We found that Cav3s are also required for proper NTC in the amphibian *Xenopus* suggesting a conserved function among chordates. Loss of Cav3 leads to defects in anterior NTC characterized by the brain protruding from the larval head. Here, I present a study expanding these findings to a new Cav3 mutant in the related species *C. robusta*. RNAseq analysis of *bugeye* mutants from both species reveals misregulation of several

transcripts including ones that are involved in cell-cell recognition and adhesion. Two in particular, *Selectin* and *Fibronectin leucine-rich repeat transmembrane protein* are aberrantly upregulated in the mutant. They are expressed in the closing neural tube and knockdown of either in wildtype larvae phenocopies the *bugeye* mutant. We speculate that these molecules play a transitory role in tissue separation and adhesion during NTC, and the failure to downregulate them properly leads to an open neural tube. One hypothesis surrounding Cav3's role in NTC, is that it acts as a mechanical developmental checkpoint, detecting the completion of NTC and signaling through calcium to move on to the next developmental process. To further explore this, I used various pharmacological inhibitors as well as manual disruption of the progression of NTC to recapitulate the open brain phenotype. The RNAseq investigation revealed a suite of transcripts that are abnormally upregulated in the *bugeye* mutant, but their expression during normal development declines sharply following neurulation. Other transcripts displaying similar expression profiles may play a role in NTC. Using publicly available RNA-sequencing data I identified several additional candidate genes. Further work is necessary to determine what role these genes play in NTC, but this demonstrates a valid approach for identifying genes with roles in specific developmental processes in *Ciona.*

TABLE OF CONTENTS

## I. Introduction

It was the late Lewis Wolpert who famously (at least among developmental biologists) stated that, “It is not birth, marriage, or death, but gastrulation which is truly the most important time in your life.” As a young developmental biologist, I have come to appreciate the complexity of the developing embryo and the number of steps it takes to reach its fully formed state. Each of these processes has a fragileness to it in the sense that a mistake at any point along the way could lead to catastrophic effects. Yet, this contrasts with a robustness that allows for faithful reproduction and development of an organism time and time again. During the early stages of embryogenesis, each process is vitally important, but if gastrulation is indeed the most important time in your life, then I would argue that neurulation is a close second. This is the subject of this dissertation in which I examine the molecular mechanisms underlying neurulation in a marine invertebrate chordate, *Ciona.*

Neurulation, or neural tube closure (NTC), is a crucial process in the development of all chordates (Nikolopoulou et al., 2017; Wilde et al., 2014). During gastrulation a flat neural plate forms on the surface of the embryo. This flat plate will be transformed into a hollow tube and form the rudimentary compartment that will eventually become the central nervous system of the embryo. While this may seem like a relatively simple process, neural tube formation is a highly orchestrated series of events that involves dramatic movement of tissue, tight coordination between many cellular and molecular

processes, and considerable interactions between the neural ectoderm and the surface ectoderm (Wilde et al., 2014).

Failure of this process during early embryogenesis accounts for a major class of human birth defects known as neural tube defects (NTDs) (Greene and Copp, 2014). These defects occur in 1 out of every 1000 pregnancies worldwide (Wallingford et al., 2013; Zaganjor et al., 2016). NTDs can range in severity, and can selectively affect the brain, the spinal cord, or both. When the neural tube fails to close in the developing brain, the neural tissue remains of the surface and eventually undergoes degradation. This leads to an open brain phenotype known as exencephaly, or anencephaly upon degradation of the neural tissue, and leads to death at or before birth (Wilde et al., 2014). When the neural tube fails to close in the spinal cord (myelomeningocele or spina bifida) the outcomes are better, but can still lead to increased infant mortality or life-long disabilities and complications (Wilde et al., 2014).

Many NTDs in humans are thought to be multifactorial with not only genetic contributions, and perhaps disturbances in more than one gene, but also environmental contributions. The most notable example of this is the contribution of maternal folate. It was noted as early as the 1950s that folate deficiency is a risk factor for early fetal death (Thiersch, 1952; Thiersch and Philips, 1950). Since then, it has been shown that supplementation with folic acid (FA) before conception and during pregnancy significantly reduces the risk of having an NTD-effected pregnancy (Czeizel and Dudás, 1992), and is now the official recommendation of the US Centers for Disease Control and Prevention (Cent.

Dis. Control Prev., 1992). As a result, the incidence of NTDs in the United States has decreased by nearly 20% (Obican et al., 2010). Despite these advances, NTDs remain one of the most common form of human birth defects highlighting the importance of understanding the genetic underpinnings of this process.

The underlying details of NTC vary from species to species (Harrington et al., 2009), however there are several mechanisms involved in the process that are broadly conserved and essential for NTC. Animal models have been used to identify over 300 genes that are critical for NTC (Wilde et al., 2014), many of which play a role in these important mechanisms. Mutations in genes encoding components of these mechanisms lead to NTDs. One important mechanism that takes place during NTC is the generation of apically polarized constrictions in the medial neural plate cells (Davidson and Keller, 1999). This allows for the bending of the neural plate and subsequent formation of the neural folds. Disruption of these actin microfilament constrictions have been demonstrated to cause particularly severe defects in the closure of the brain (Ybot-Gonzalez and Copp, 1999), but can also affect the closure of the spinal cord (Haigo et al., 2003). Another major mechanism involved in NTC is convergent extension (CE). This allows the embryo to lengthen along the rostral-caudal axis and narrows the neural plate (Wallingford, 2012; Ybot-Gonzalez et al., 2007). This process is largely controlled by the planar cell polarity (PCP) pathway, and mutations in various PCP proteins, such as *dishevelled* and *vangl2,* disrupt these critical cell movements. In animal models these mutations have been shown to give rise to some of the most severe NTDs, including craniorachischisis in which the entirety

of the neural tube remains open from the brain to the spinal cord (Wilde et al., 2014). Several PCP pathway mutations have been directly associated with similar NTDs in humans (Juriloff and Harris, 2012; Robinson et al., 2012).

The final step in NTC is the fusion of the neural folds across the dorsal midline. Here the once contiguous neuroepithelium (NE) and non-neural ectoderm (NNE) must separate and fuse creating two separate structures: the inner neural tube covered by the outer NNE, which will go on to develop as the epidermis (Copp et al., 2003). Some key factors have been identified in this process, such as Grhl2 and N-cadherin (Bronner-Fraser et al., 1992; Pyrgaki et al., 2011), but there remains much unknown regarding the sealing of the neural folds.

The process of neurulation is shared among chordates; however, in vertebrates, NTC is a highly complex process under the control of a plethora of genes (Nikolopoulou et al., 2017) and the complexity of these higher organisms may obscure genetic components controlling NTC that have yet to be elucidated. It is here where turning to the simplest of chordates may give us further insight into some of the veiled mechanisms controlling this process. My research has focused on the ascidian *Ciona,* and before I describe the process of interest, neurulation, I would like to spend some time explaining the characteristics of *Ciona* that make it an ideal organism to study chordate developmental processes in general.

*Ciona* are members of the chordate clade Tunicata and as such they share the chordate body plan, including a notochord and a dorsal hollow neural

tube (Passamaneck Yale J. and Di Gregorio Anna, 2005). In their larval form, the tunicates have a body plan much like that of vertebrates. In fact, they are the sister group with the clade Vertebrata, making them the closest living relative of the vertebrates (Delsuc et al., 2006). They are sessile marine invertebrates that filter feed and attach to rocks, shells, and pilings (Holland, 2002). Conveniently, they also attach to the bottom of boats and other objects floating in the Santa Barbara Yacht Harbor, making them easy to collect. The adult body is covered by a thick covering made of cellulose called a tunic (Nakashima et al., 2004). They are hermaphrodites with distinct ducts containing sperm and eggs allowing for specific crosses to be performed with simple dissection under a benchtop stereo microscope (Satoh, 2003).

The fertilized eggs of *Ciona* undergo bilaterally symmetric cleavage in a highly determinate pattern. When the embryo reaches 112 cells it will undergo gastrulation, followed by neurulation, after which tailbud embryos grow into a mature tadpole that will hatch from its chorion, all within 18 hours at 18°C (Hotta et al., 2007; Lemaire, 2009). This means the entire process of neural tube closure occurs within in a span of 2 hours at 18°C. This relatively simple tadpole consists of only around 2600 cells, but contains a distinct epidermis, central and peripheral nervous system, endoderm, notochord, muscle, and mesenchyme (Passamaneck Yale J. and Di Gregorio Anna, 2005). Tunicate larvae will swim and then attach to a surface using an adhesive organ called the palps, undergo metamorphosis, and give rise to adults in sometimes as little as 2-3 months given the environmental conditions (Satoh, 2013).

Not only do the embryos of *Ciona* contain a limited number of cells, but the lineage of each cell is known. At the 8-cell stage the distinct axes are present and each cell is given a unique number. The anterior cells are given the “a” distinction with posterior cells given “b”. Those on the ventral side are given lowercase distinctions “a” and “b” while those on the dorsal side are given uppercase distinctions “A” and “B” (Conklin, 1905; Ilsley et al., 2020). It is largely the a- and A-line cells that will give rise to the nervous system, with contributions from the b-line as well (Hudson, 2016) (Figure 1.1A). In *Ciona*, neural induction begins at the 32-cell stage and continues through gastrulation in which the neural plate forms on the surface of the embryo. The neural plate consists of about 44 cells arranged in a grid-like pattern with 6 rows and 5 bilaterally symmetric columns (Hudson, 2016) (Figure 1.1B). Signaling through Nodal, Delta2/Notch, and FGF/MEK/ERK in both a sequential and combinatorial manner establish the individual identities of neural plate cells (Hudson et al., 2007). Most of the cells are destined to give rise to a particular tissue or organ by gastrulation (Nishida, 1987). By the 112-cell stage, 102 blastomeres are restricted to a particular fate (Satoh, 2013).

In the larval stage, the central nervous system consists of about 180 neurons and about 330 total cells with the remainder largely consisting of ependymal (glial) cells (Ryan and Meinertzhagen, 2019). It is divided into several regions including the sensory vesicle, posterior brain, neck, visceral ganglion, and nerve cord (Hudson, 2016; Imai et al., 2009) (Figure 1.1C). Inside the sensory vesicle there are two pigment spots. One is associated with the otolith, a

gravity-sensing organ and the other is associated with the ocellus which is a light-sensing organ (Bostwick et al., 2020) (Figure 1.1C).

In 2002, the first draft of the *C. intestinalis* genome was published (Dehal et al., 2002). It identified many of the developmentally relevant genes used by vertebrates, without the redundancy resulting from two genome-wide duplications in the vertebrate lineage, making it easier to elucidate the functions of individual genes involved in developmental processes (Kasahara, 2007). The genome for a second *Ciona* species, *C. savignyi*, was also sequenced (Small et al., 2007; Vinson et al., 2005). Due to the having a high-level of allelic polymorphisms, with 1.2% of the nucleotides differing between alleles in *C. intestinalis* and an even higher percentage differing in *C. savignyi*, wild populations of the two species provide an abundant source of naturally occurring mutants (Veeman et al., 2011).

Previously, the Smith lab took advantage of this fact to screen for spontaneous mutants and identified a recessive line of *Ciona savignyi* with an open brain phenotype (*bugeye*). This mutant was mapped to a mutation in the gene for a T-type calcium channel *Cav3* (Abdul-Wajid et al., 2014). Cav3, as a T-type calcium channel, is a part of a family of low voltage-activated channels that act transiently (Wang et al., 2009). They have various functions including contributions to electrical activity in neurons and synaptic transmission. Defects in activity of these channels are associated with many disorders including neuropathic pain and epilepsy (Weiss and Zamponi, 2019). They are thought to have a key role in amplifying and integrating signals rather than necessarily

being the initiator of the signal (Gray et al., 2013; Leresche and Lambert, 2017; Wang et al., 2009).

Loss of Cav3 results in failure of NTC characterized by the brain protruding from the larval head, similar to exencephaly. These mutants display no defects in neural induction or neural fold formation, but rather in neural fold fusion. Experiments in *Xenopus* showed a conserved requirement for Cav3 in NTC, suggesting it plays a role in all vertebrates (Abdul-Wajid et al., 2015).

Loss of this channel in *Ciona* is accompanied by upregulation of *EphrinAd,* a member of the Eph/Ephrin family, through which signaling has been reported to promote fusion of the neural folds (Abdul-Aziz et al., 2009). Ephs can be involved in both cell adhesion and repulsion depending on the context (Arvanitis and Davy, 2008; Holmberg et al., 2000). In wildtype *Ciona* embryos, *EphrinAd* is downregulated following NTC and this downregulation is required for proper closure of the anterior neuropore (Abdul-Wajid et al., 2015).

This led to the hypothesis that signaling through Cav3 may regulate the expression of a host of genes required for neural fold fusion and completion of NTC, and that this may involve promotion of adhesion across the neural folds and/or elimination of repulsive signals.

The first chapter of this dissertation will focus on the work to further elucidate the mechanisms of neural tube closure (NTC) in the *Ciona* T-type calcium channel Cav3 mutant, *bugeye,* through RNA-sequencing of two species (*C. robusta* and *C. savignyi*) to identify additional misregulated transcripts that may play a role in the fusion of the neural folds.

Next, I will discuss work that further examines the *bugeye* mutant. I address one particular challenge to working with this mutant - the fact that the appearance of the open brain phenotype does not occur until later in its development, much past neurulation, despite the fact that inhibiting Cav3 during NTC is the optimal time for producing the phenotype.

Finally, I will describe the initial work of a project developed based off the idea that many of these genes we were looking at show a sharp decrease in expression soon after the completion of NTC. Using publicly available RNA-sequencing data of *Ciona* across several stages of development, I identified other genes with a sharp decrease in expression following neurulation. Further analysis shows that this may be a valid way to discover novel roles for genes in a specific developmental process in *Ciona.*

## Figures

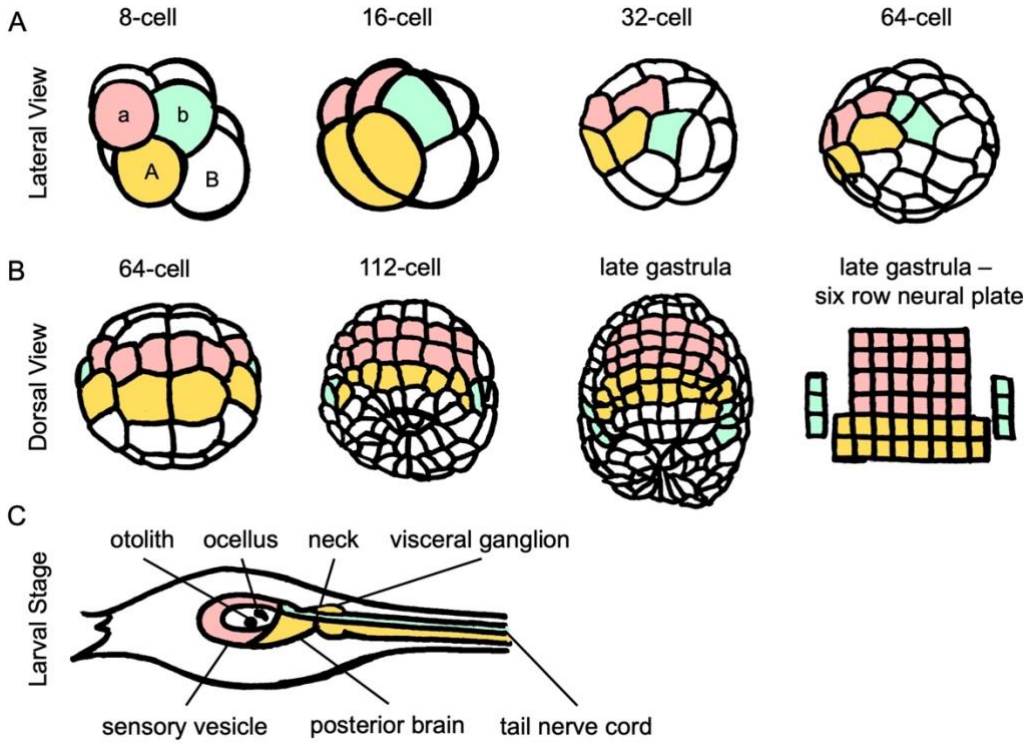


**Figure 1.1. Cell lineages of the *Ciona* central nervous system. A.** Lateral view of embryos from the 8-cell stage to the 64-cell stage. **B.** Dorsal view of embryos from the 64-stage to the six-row neural plate stage. **C.** Organization of the central nervous system of larval *Ciona.* Embryos from the 32-cell stage to the late gastrula stage were adapted from 3D renderings of *Ciona* embryos on the web-based anatomical browser MorphoNet (https://morphonet.org/). Coloring of cell lineages was adapted from Hudson (2016) and the images on MorphoNet.

## II. Misregulation of cell adhesion molecules in the *Ciona* neural tube closure mutant *bugeye*

The following chapter of this thesis is from my article published in the December 2021 issue of *Developmental Biology*. I would like to acknowledge the contributions from the other authors, in particular, the significant work done by Stephanie M. Khairallah on the *C. robusta bugeye* mutant mapping and by Erin Newman-Smith in analyzing the RNA-sequencing results.

### A. Abstract

Neural tube closure (NTC) is a complex multi-step morphogenetic process that transforms the flat neural plate found on the surface of the neurula embryo into the hollow and subsurface central nervous system (CNS). Errors in this process underlie some of the most prevalent human birth defects and occur in about 1 out of every 1000 births. Previously, we discovered a mutant in the basal chordate *Ciona savignyi* (named *bugeye*) that revealed a novel role for a T-Type Calcium Channel (Cav3) in this process. Moreover, the requirement for Cav3s in *Xenopus* NTC suggests a conserved function among the chordates. Loss of CAV3 leads to defects restricted to anterior NTC, with the brain apparently fully developed, but protruding from the head. Here we report first on a new Cav3 mutant in the related species *C. robusta*. RNAseq analysis of both *C. robusta* and *C. savignyi bugeye* mutants reveals misregulation of a number of transcripts including ones that are involved in cell-cell recognition and adhesion. Two in particular, *Selectin* and *Fibronectin leucine-rich repeat transmembrane protein,*

which are aberrantly upregulated in the mutant, are expressed in the closing neural tube, and when disrupted by CRISPR gene editing lead to the open brain phenotype displayed in *bugeye* mutants. We speculate that these molecules play a transient role in tissue separation and adhesion during NTC and failure to downregulate them leads to an open neural tube.

## B. Introduction

Neurulation is a defining morphogenic event of the chordates and results in the characteristic dorsal and hollow central nervous system (CNS) (Nikolopoulou et al., 2017; Wilde et al., 2014). The CNS starts as the flat neural plate from which the neural folds form at the lateral edges as cells there undergo apical constriction. Convergence and extension within the neural plate bring the lateral neural folds together where they meet and fuse, forming the neural tube. Failure at any one of the many steps of this process can result in neural tube defects (NTDs). These defects range in severity and can specifically target the developing spinal cord or brain, or both. Often, NTDs can be traced back to disruption of specific cellular events during neural tube closure (NTC), such as apical constriction (Ybot-Gonzalez et al., 2007), convergent extension (Murdoch et al., 2001; Wallingford and Harland, 2001), and/or neural fold adhesion (Bronner-Fraser et al., 1992; Pyrgaki et al., 2011). However, there is still much to be learned about the underlying mechanisms controlling these defects. Together NTDs are the most common and debilitating form of human birth defects, occurring in approximately 1 out of every 1000 births (Copp et al., 2013).

The ascidians of the genus *Ciona* offer a uniquely simple model to study the process of neural development, including NTC. *Ciona*, and the other members of the tunicate clade of invertebrate chordates, are the closest living relatives to vertebrates and share a stereotyped chordate body plan (Lemaire et al., 2008). However, the *Ciona* larva is much simpler than similarly-staged vertebrates, consisting of only about 2600 cells, and has a fixed lineage during embryogenesis (Hotta et al., 2007). The neural plate in *Ciona* consists of only 40 cells arranged in a grid-like pattern [reviewed in (Hudson, 2016)]. Neurulation in *Ciona*, and other tunicates, follows a vertebrate-like sequence with the neural folds meeting along the dorsal midline and then closing in a zipper-like manner from the posterior end to the anterior end (Hashimoto et al., 2015). Final closure of the anterior neuropore occurs via a purse-string mechanism, coordinated by the constriction of cells at their apices. In *Ciona*, this entire process follows a stereotyped pattern of cell division and is complete in less than two hours (Hotta et al., 2007; Nicol and Meinertzhagen, 1988a, 1988b).

We previously identified a recessive mutant line of *Ciona savignyi* we named *bugeye (bug)* in which the neural folds fail to close in the brain, resulting in an exencephaly-like phenotype (Abdul-Wajid et al., 2015). This mutant line revealed a role for the T-Type $Ca^{2+}$ Channel Cav3 in NTC. Neural plate induction and differentiation appear to occur normally in *bug* mutants. Proper neural folds appear to form and close in the posterior CNS, while the anterior neuropore remains open. Time-lapse movies show that in *bug* animals the brain is subsurface by the end of the neurula stage, but in the next few hours erupts from

the anterior neuropore. The precise role Cav3 plays in the *bug* phenotype is unclear. However, based on the observed misregulation of transcripts, we hypothesized that Cav3 plays an essential regulatory role in fusion of the anterior neural folds - perhaps in monitoring the progression of NTC. Morpholino knockdown of an orthologous gene in *Xenopus*, Cav 3.2, also leads to an open brain (OB) phenotype suggesting that Cav3s have conserved functions in NTC across the chordate clade (Abdul-Wajid et al., 2015).

The *bug* mutant provides a tool for studying a poorly characterized step of NTC: the adhesion and final sealing, of the edges of the forming neural tube. These final steps are a complex junctional exchange that involves both the separation of the forming neural tube from the adjacent epidermis, and the cell-cell recognition and subsequent adhesion of the edges of the closing neural plate and overlying epidermis. Much remains unknown regarding this final step in NTC. Early work in this area made key observations revealing the importance of deposition of extracellular matrix molecules and subsequent formation of the basal lamina in the separation of these two tissues (Martins-Green, 1988). In addition to the importance of ECM deposition, cellular protrusions have been shown to be a key aspect of neural tube closure in vertebrates (Davidson and Keller, 1999; Geelen and Langman, 1977, 1979; Massarwa and Niswander, 2013; Pyrgaki et al., 2010). These protrusions span the midline gap and are the first point of contact between the two folds, although their functions are not fully understood (Nikolopoulou et al., 2017).

Loss of *Cav3* function in *bug* mutants is accompanied by upregulation of EphrinAd, a member of the ephrin cell-adhesion/repulsion family. In addition to Ephrin's, other cell adhesion and repulsion molecules are known to be important in NTC, including NCAM, N-cadherin, nectin-2, and E-cadherin (Bronner-Fraser et al., 1992; Deak et al., 2005; Suzuki et al., 2012). In this report, we use the *bug* mutant in *Ciona* to find additional factors involved in NTC using RNAseq analysis. With this strategy we identified additional cell adhesion/repulsion molecules that, like EphrinAd, are differentially expressed in *bug* versus wild type (WT) embryos. We find that two in particular, *L-Selectin (Sel)* and *Fibronectin leucine-rich repeat transmembrane protein* (*Flrt*), are highly upregulated in *bug* mutants. Overexpression and CRISPR gene editing experiments demonstrate that both of these genes are essential for normal NTC.

## C. Methods

### Animals

*Ciona robusta* were either collected from the Santa Barbara Harbor, or were ordered from M-REP (Carlsbad, CA). *Ciona savignyi* were collected from the Santa Barbara Harbor. The mutants *C. robusta bug* and *C. savignyi bug* were cultured at the UC Santa Barbara Marine Lab, as previously described (Veeman et al., 2011). Embryos and larvae were obtained by dissecting gametes from 2-3 adults and culturing them in natural seawater at 18°C, or by natural spawning (Veeman et al., 2011).

### *Ciona robusta bug* mutation

For the complementation test, *C. robusta bug* eggs were first dechorionated (Veeman et al., 2011; Zeller, 2018) to allow for cross-species fertilization, and then were mixed with either *C. robusta bug* sperm or *C. savignyi bug* sperm. The resulting embryos were then analyzed for the *bug* phenotype at late tailbud stage. For linkage analysis, *C. robusta bug* and WT sibling larvae genomic DNA was collected as previously described (Veeman et al., 2011). Primers used to sequence the intronic region of Cav3 are listed in Supplemental Table 2.2. For cDNA and RT-PCR analysis, *C. robusta bug* larvae RNA was extracted and cDNA generated as previously described (Abdul-Wajid et al., 2014). Cav3 RT-PCR and cDNA cloning primers are listed in Supplemental Table 2.2. For cDNA sequencing, Cav3 cDNA amplicons were TA-cloned into pCR8 vector using pCR8/GW/TOPO TA Cloning Kit (Invitrogen). Cav3 cDNA was sequenced using M13 forward primer, T7 forward primer, or internal primers listed in Supplemental Table 2.2. All sequencing was performed by UC Berkeley DNA Sequencing Facility. *C. robusta* Cav3 WT transmembrane structure was manually plotted and visualized by Protter (http://wlab.ethz.ch/protter/) (Omasits et al., 2014).

### RNAseq

Three samples of approximately 200 embryos each were collected from 3 separate fertilizations. Hatched larva embryos (24 hours post fertilization at 18°C)

with the *bug* phenotype and their wild-type siblings from a cross of 4 *C. robust*a or *C. savignyi* heterozygous *bug* adults were collected on ice and washed twice in $H_2O$. Follicle cells, which are maternally-derived, were removed with 0.5M EDTA and gentle pipetting (Veeman et al., 2011). RNA was prepared using the NucleoSpin RNA XS kit (Macherey-Nagel). Library preparation and sequencing were performed at the Genetics Core of the California Nanostructures lab at UCSB. cDNA libraries were prepared using the TruSeq Stranded mRNA Library Prep kit (Illumina) and barcoded for each pooled RNA sample. High-throughput paired-end sequencing was performed using the Illumina NextSeq 500 sequencer generating maximum reads of 150 nucleotides and a read depth of 37-63 million reads/sample. *C. robusta* data was analyzed using the STAR alignment program to align reads to the *C. robusta* genome (Dobin et al., 2013). The number of reads per mRNA was determined using the Partek Genomics Suite (Partek Inc.). Differential expression analysis and statistical tests were performed using edgeR (McCarthy et al., 2012). *C. savignyi* sequence was aligned to the reference genome with HiSat and gene level counts determined with StringTie (Pertea et al., 2016), but edgeR was used to determine differential expression and perform statistical tests, as above. We identified (using an FDR < 0.05 as a cutoff) 6 genes in *C. savignyi* and 33 in *C. robusta* that were upregulated, and 22 genes in *C. savignyi* and 39 genes in *C. robusta* that were downregulated, in *bug* mutants (Supplemental Table 2.1).

## Transcript analyses

**End point PCR.** RNA was extracted from wild-type and *bug* larvae using the NucleoSpin RNA XS kit (Macherey-Nagel). With this template cDNA was synthesized using the SuperScript IV First-Strand Synthesis System (Invitrogen). RT-PCR was performed with the primers listed in Supplemental Table 2.2 (RT-PCR primers). Following agarose gel electrophoresis, the results were quantified and analyzed using FIJI (Schindelin et al., 2012).

**RT-qPCR.** Hatched larva embryos (24 hours post fertilization at 18°C) were washed twice in distilled $H_2O$ and RNA was isolated using the NucleoSpin RNA XS kit (Macherey-Nagel). RNA was reverse transcribed using SSIV reverse transcriptase (Invitrogen) and random hexamer primers following the manufacturer's protocol. cDNA was amplified using SYBR-green polymerase Master Mix (Thermo Fisher Scientific) and indicated primers (see Supplemental Table 2.2). Samples were run on a BioRad CFX96 Real-Time System PCR machine. Samples were run in triplicate from three independent CRISPR/Cas9 experiments. *Sel* expression levels are relative to actin and RPS27A and were determined using the ddCT method and R program ddCT (Zhang et al., 2020).

### Hybridization chain reaction (HCR) *in situ*

HCR in situs were performed as described previously (Kourakis et al., 2019). Briefly, *Ciona robusta* were fixed in 4% paraformaldehyde at various

time points using the published staging guide (Hotta et al., 2007). HCR *in situ* probes for *Flrt* (KH.C6.163) and *Lphn* (KH.C5.597) were obtained from Molecular Technologies. Sequences are available from the Aniseed website (aniseed.cnrs.fr) using the KH gene model. The larvae were cleared with Slowfade Gold with DAPI (Invitrogen) and imaged on an Olympus FLUOVIEW FV1000 confocal laser scanning microscope and visualized using Imaris (Bitplane).

**DNA constructs**

Genomic DNA was isolated as previously described (Veeman et al., 2011) from *C. robusta* tailbud embryos. Promoter sequences of *lncRNA* (Kh.C11.667), *SoxE* (KH.L154.42) and *Sel* (KH.C1.372) were PCR amplified (Expression construct primers, Supplemental Table 2.2) and cloned into the Gateway entry vector pCR8/GW/TOPO vector (Invitrogen), and then recombined into the final destination vector p1.72BSSPE/ISce1/RfA:H2B:EGFP, containing an eGFP gene fused to H2B histone gene (Auger et al., 2009). Embryos were electroporated as described below. Embryos were fixed and immunostained using primary antibodies against GFP and RFP (Life Technologies Corp.). Washing, secondary staining and clearing were as described (Veeman et al., 2011).

A full length *Flrt* cDNA was amplified from clone cima898007 (Gilchrist et al., 2015) using Q5 polymerase (NEB), A-tailed by incubation with GoTaq (Promega), and cloned into the pCR8/GW/TOPO TA entry vector. This entry

vectors along with an entry vector containing the OTX promoter region were recombined into the final destination vector pSP72BSSPE-R3-ccdB/cmR-R5::RfA (Roure et al., 2007) generating OTX>Flrt. Similarly, RFP cDNA was amplified from a *Ciona* expression optimized RFP construct (Zeller et al., 2006)**,** using the same protocol to generate OTX>RFP. CRISPR/Cas9 constructs were generated following the protocol in (Stolfi et al., 2014). sgRNA sequences were selected using CRISPOR (Concordet and Haeussler, 2018), and are listed in Supplemental Table 2.2.

**Electroporation**

Electroporations into *C. robusta* were performed as described previously (Veeman et al., 2011; Zeller, 2018). Embryos were electroporated with 40µg of the expression or overexpression constructs. For overexpression embryos were co-electroporated with 15µg of ETR>H2B:GFP (Veeman et al., 2010) to mark the nervous system. Following electroporation embryos were cultured in filtered sea water with antibiotics at 18°C until they reached the hatching stage (Veeman et al., 2011). Embryos were scored for phenotype, fixed, and imaged (Veeman et al., 2011).

For CRISPR/Cas9 experiments, embryos were dechorionated using 0.1% Trypsin (Sigma T4799) in 10mM TAPS pH 8.2 in filtered sea water as described in (Sardet et al., 2011). Embryos were electroporated with 25µg of each of two sgRNA constructs, except with *Flrt*, for which 50 µg of plasmid was used (sgRNA sequences listed in the Supplemental Table 2.2). The previously published control sgRNA is a sequence not found in the *Ciona* genome (Stolfi et al., 2014).

The sgRNAs were co-electroporated with 32 µg EF1$\alpha$ Cas9 (Stolfi et al., 2014), as well as 15 µg of pBRA>h2bRFP, to serve as a control for electroporation efficiency (Kourakis et al., 2014). Embryos were cultured in 0.2% methylcellulose in filtered sea water on 1% agarose-coated petri dishes at 18°C for 23-25 hours. Hatched larva embryos were anesthetized with 0.04% MS-222 (Sigma) and the neural tube scored as open or closed.

### DNA sequencing to detect genomic editing in CRISPR animals

To assess the efficiency of CRISPR/Cas9 genome editing, DNA was isolated from pools of either OB or CB embryos for each sgRNA using the QIAmp DNA Micro Kit (Qiagen). Sequences were PCR amplified around the sgRNA site and Sanger sequenced by the UC Berkeley DNA Sequencing Facility. Primer sequences are shown in the Supplemental Table 2.2.

## D. Results

### A *C. robusta Cav3* mutant

During a screen for spontaneous developmental mutants in *C. robusta* (Veeman et al., 2011), we identified a mutant line with a recessive OB phenotype similar to that of the *C. savignyi* mutant *bug* (Abdul-Wajid et al., 2015). To characterize this mutant (provisionally named *open brain, ob*), we performed a complementation test between *C. savignyi bug* and the *C. robusta ob*, as described previously for complementation tests between *Ciona* species (Salas et

al., 2018). Dechorionated eggs from a heterozygous *C*. *robusta ob* were crossed with sperm from a heterozygous *C*. *savignyi bug*. The dechorionated *C*. *robusta ob* eggs were also crossed with *C*. *robusta ob* sperm. As a control, wild type (WT) sperm and eggs were used. For crosses using gametes from the *ob* and *bug* adults, the OB phenotype was observed at the approximate percentages expected for non-complementing recessive mutations [31% for *C. robusta ob* x *C. savignyi bug* (n = 53), and 26% for *C. robusta ob* x *C. robusta* ob (n =55)], while the occurrence of OB was very low in the negative controls (Figure 2.1A). Representative images of the OB phenotypes from both crosses are shown in Figure 2.1B. The complementation test results are consistent with *ob* and *bug* being lesions in the same genes of their respective species.

To further investigate the *ob* locus, it was tested for linkage to the *C. robusta Cav3* gene using intronic allelic-specific single nucleotide polymorphisms (SNPs), as described previously (Veeman et al., 2011). Two *C. robusta* adults heterozygous for *ob* were crossed, and genomic DNA was collected from pools of 20 OB larvae, and 20 closed brain (CB) larvae, which would contain a mixture of homozygous WT and heterozygous siblings. A fragment from the 16th intron of *Cav3* was PCR amplified from the two pools and sequenced. Figure 2.1C shows a segment of the intron sequence containing a SNP observed in the CB pool (arrow). However, in the genomic DNA pool from the OB progeny only one allele is present (arrow), consistent with this allele of *Cav3* being linked to the causative mutation. Taken together, the similarity of *ob* phenotype to *C. savignyi bug*, and the complementation and linkage results, lead us to conclude that the *C. robusta*

*ob* mutation is in the same gene as *C. savignyi bug*, and will be called from here on *C. robusta bugeye (bug)*.

In *C. savignyi bug*, *Cav3* has an 83 bp insertion in the promoter region that we hypothesized results in the observed under expression of *Cav3* (Abdul-Wajid et al., 2014). By contrast, we did not observe a decrease in *Cav3* mRNA levels in *C. robusta bug* larvae by RT-PCR (Figure 2.1D). We sequenced *Cav3* cDNA from *C. robusta bug* and found multiple amino acid changes throughout the sequence in comparison to the published sequence (XP_018667819.1) (Figure 2.1D). To characterize these amino acid substitutions, the predicted amino acid sequence for WT *Cav3* was mapped to the known transmembrane topology of *Homo sapiens* CAV3.2 (Figure 2.1E). Many of the amino acid substitutions in the *C. robusta bug* Cav3 are in regions of known functional importance. Notably, a majority of the amino acid changes (2-5, Figure 2.1E) are found in the I-II loop, which is important for proper membrane expression and channel gating of CAV3.2 (Vitko et al., 2007; Zhang et al., 2013). There is also a non-conserved amino acid substitution (T2126I, number 6 in Figure 2.1E) in the C-terminal tail, a region which is important for CAV3 regulation and interactions with other proteins for downstream events (Anderson et al., 2010; Asmara et al., 2017; Jurkovicova-Tarabova et al., 2019; Weiss et al., 2012). We suspect that the multiple mutations in functional regions of the *C. robusta bug Cav3* likely lead to improper function of Cav3.

**RNA transcriptome sequencing of *bug* mutants reveals mis-regulated transcripts**

We previously reported that *EphrinAd* was upregulated in homozygous *C. savignyi bug* larvae (Abdul-Wajid et al., 2015). We hypothesized that the failure of NTC leads to the abnormal persistence of genes that would otherwise be downregulated at the completion of NTC. To find other genes that follow this pattern, and to identify potential new components of the NTC machinery, we performed deep sequencing of RNA (RNAseq) from homozygous *bug* larvae and their phenotypically WT siblings. This was done for both the original *C. savignyi bug* isolate, as well as the new *C. robusta bug* mutant. We identified 6 genes in *C. savignyi* and 33 in *C. robusta* that were upregulated in *bug* mutants, and 22 genes *C. savignyi* and 41 in *C. robusta* bug mutants that were downregulated (Supplemental Table 2.1; FDR < 0.05 threshold). While *bug* mutants from both species have similar phenotypes and are linked to *Cav3*, non-overlapping lists of differentially expressed genes were generated, suggesting that the screens were not saturating. Consistent with this, we did not detect reduced expression of *Cav3* in *C. savignyi* RNAseq data, which has been shown by qRT-PCR to be downregulated in *bug* mutants (Abdul-Wajid et al., 2015). Moverover, *Cav3* is expressed at very low levels, and we would likely need many more replicates of *bug* and WT RNA to have the statistical power to find differential expression in rare transcripts.

Among the upregulated genes identified in the RNAseq analysis are some with known roles in NTC (Supplemental Table 2.1). For example, *Homeodomain*

*interacting protein Kinase 2* (*Hipk2*) is a member of a nuclear serine/threonine family of kinases, and when knocked out in the mouse (with *Hipk1*) results in a failure of the anterior neuropore to close, leading to exencephaly (Isono et al., 2006). The *solute carrier family 25 (SCF25)* encodes mitochondrial membrane transport proteins. One member, *SCF25A32*, is a folate transporter, and a mouse null mutant at this locus dies *in utero* with neural tube defects (Kim et al., 2018). *Bone morphogenic protein (BMP)* regulates NTC by maintaining the stability of the neural epithelium, and a decrease in BMP is required for the formation of the neural folds (Eom et al., 2011). The RNAseq data also show an upregulation of the FGF receptor. In vertebrate embryos, *Fgf3* regulates *Bmp* in the neuroepithelium (Anderson et al., 2016), and in *Ciona, FGF* is necessary for the normal morphogenesis of the neural tube (Navarrete and Levine, 2016). However, the majority of the genes on our list have not been implicated previously in NTC.

As an initial validation of the RNAseq results, we performed RT-PCR on several upregulated genes including the most-up regulated from each species, *L-Selectin* (*Sel*) and *Flrt*. We also validated RNAseq results from two other genes, *SoxE* and a long non-coding RNA called here *lncRNA,* which have lower levels of upregulation (log fold change values of 1.09 and 0.86 respectively, Supplemental Table 2.1). *Sel*, *SoxE*, and *lncRNA* had not previously been associated with NTC. However, *Flrt* has been shown to give an OB phenotype when knocked out in mice (Maretto et al., 2008), but its role in NTC has not been studied in detail. We measured levels of transcript from the target genes in *C. robusta bug*

mutants using RT-PCR. *lncRNA*, *SoxE* and *Sel* were expressed at higher levels in. *C. robusta bug* larvae than in WT siblings (Figure 2.2A), as well as *Flrt*, which was initially identified in *C. savignyi*.

We examined the spatial expression of these four genes with the expectation that the target genes identified in the RNAseq screen should be expressed in, or surrounding, the closing neural tube. For this analysis the promoter regions of *lncRNA*, *Sel*, *SoxE* of were isolated and inserted into an enhanced Green Fluorescent Protein (eGFP) expression plasmid (Figure 2.2B). An expression construct was also made for *Ependymin (Epd),* a gene downregulated in *C. robusta bug* mutants (Supplemental Figure 2.1). The expression of *Flrt* was characterized by *in situ* hybridization, rather than by transgenesis, in order to investigate co-expression with its binding partner Latrophilin (Lphn) (see below). We also attempted *in situ* hybridization for *lncRNA*, *Sel*, *SoxE*, using the highly sensitive hybridization chain reaction method (Choi et al., 2018), but were unable to detect a specific fluorescent signal. The expression constructs were co-electroporated with a construct containing the pan-neural marker *ETR-1* driving nuclear red fluorescent protein in order to label the CNS (Satou et al., 2001). At early tailbud-stage, all constructs were observed to be expressed in the closing anterior CNS (arrows, Figure 2.2B). In addition, the *lncRNA, Sel* and *SoxE* constructs are expressed in the developing palps, which derive from non-neurulating neural plate (arrowheads) (Veeman et al., 2010). These results confirmed that our RNAseq strategy is able to identify genes expressed in the closing neural tube.

We hypothesize that completion of NTC serves as a signal to downregulate the expression of a number of genes in the newly closed neural tube, in particular those involved in cell recognition and adhesion, such as *Ephrin Ad*, and that in *bug* embryos this signal is disrupted. Interestingly, the two highest overexpressed genes to come out of the RNAseq analysis, *Sel* and *Flrt*, also encode cell adhesion proteins. We analyzed the expression of *Flrt* and *Sel* in WT embryos over the course of development using RT-PCR (Figure 2.2C, D). Both *Flrt* and *Sel* have a peak of expression around mid-neurula (stage 15), which then decreases to very low levels during the late tailbud stage, (stage 23, 12 hours post fertilization (hpf)) and hatching stage (stage 26). This decrease in expression that occurs in normal development of *Ciona* may be impaired in *bug* mutants resulting in aberrant upregulation. This also provides correlative evidence that these two molecules are functioning during this stage of development.

**OB caused by multiple pathways results in *Sel* upregulation**

Our analysis so far has been based on the Cav3 mutant *bug*, but mutations in other genes also lead to NTC failure characterized by an OB phenotype. Using the most highly upregulated transcript, *Sel,* we assayed whether this differential expression is a general feature of NTC failure by using CRISPR/Cas9 to target both *ACAM*, a gene that has been previously shown to be essential for normal NTC in *C. robusta* (Morales Diaz et al., 2016), and *NCAM*, which has also been implicated in human NTC (Deak et al.,

2005). Single guide RNAs (sgRNA) were made for *ACAM* and *NCAM* with the ubiquitous U6 promoter which expresses beginning at the 16-cell stage (Pickett and Zeller, 2018; Sasaki et al., 2014; Stolfi et al., 2014). A control sgRNA-containing a sequence not found in the *C. robusta* genome was used (Stolfi et al., 2014) (see Supplemental Table 2.1 for sequences). Embryos were electroporated with these constructs along with ubiquitously expressed *Cas9,* using the *Ef1α* promoter (Sasakura et al., 2009; Stolfi et al., 2014), grown to the hatched larva stage (24 hours at 18°C) and scored for the OB phenotype. We found that sgRNAs targeting both *NCAM* and *ACAM* led to a significant increase in OB in embryos compared to animals electroporated with the control sgRNA, as well as a significant increase in *Sel* expression as detected by qRT-PCR (Figure 2.3). We also observed that spontaneous OBs occurred in our samples at a low, but variable, frequency (e.g., Figure 2.5). Additionally, the process of egg dechorionation, a necessary step in electroporation (Christiaen et al., 2009), increased the frequency of spontaneous OB. Interestingly, when these spontaneous OB embryos were assessed, they too had elevated *Sel* expression (Figure 2.3), consistent with our hypothesis that failure to close the brain leads to persistent expression of certain genes.

**Flrt is expressed during NTC**

One of the most highly upregulated genes resulting from the RNAseq analysis was *Flrt*. *Flrt* is a cell adhesion molecule with 10 extracellular leucine-rich repeats flanked by cysteine rich repeats, a single type III fibronectin domain,

and a transmembrane domain joined to a short intracellular tail (Lacy et al., 1999). We used hybridization chain reaction (HCR) *in situ* in order to more precisely examine the temporal and spatial expression of *Flrt* during NTC (Figure 2.4) (Choi et al., 2018). At mid-gastrula stage (stage 12) the developing *Ciona* neural plate is laid out in six rows of cells (Hotta et al., 2007; Hudson and Yasuo, 2005; Wagner and Levine, 2012). A stripe of *Flrt* expression was observed stretching across the middle row of cells (Figure 2.4A), corresponding to cell pairs a9.37, 9.33, and a9.49 (highlighted with box, Figure 2.4B). These cells will give rise to the anterior brain vesicle (aBV) (Cole and Meinertzhagen, 2004; Nishida, 1987). Later, at mid-neurula (stage 15), the restricted aBV pattern persists as expressing cells begin to form a ring around the future anterior neuropore (Figure 2.4C) (Hashimoto et al., 2015). As neural tube closure nears completion with the formation of the definitive anterior neuropore at the initial tailbud stage (stage 17), *Flrt* expression decreases (Figure 2.4D) as expected based on its expression over the course of development (Figure 2.2C). Thus the spatial and temporal expression pattern of *Flrt* suggests that it plays a role in brain closure, but not caudal neural tube closure, as is observed in *bug* mutants (Abdul-Wajid et al., 2015). This is consistent with analysis of NTC in ascidians, which shows that the brain and caudal neural tube use different mechanisms in closure (Hashimoto et al., 2015).

### *Flrt* and *Lphn* are expressed in opposing domains within the neural tissue

One of the most extensively studied roles for Flrt has been in its role in the process of neurite outgrowth and development. While the role of Flrt in neurite outgrowth has been extensively studied (Robinson et al., 2004; del Toro et al., 2020), its mechanism of action is complex and not fully resolved. Flrt appears to function in different contexts as either an adhesive or repulsive molecule (Seiradake et al., 2014; Yamagishi et al., 2011). Flrt can form homodimers, as well as interact with other proteins, most prominently, Lphn. Where it has been studied, Flrt and Lphn are not co-expressed in cells, but rather are observed in adjacent cells, such as across synapses or between migrating neurons (Lu et al., 2015; O'Sullivan et al., 2012). Lphn is a G-protein coupled receptor with a large adhesion-like extracellular N-terminal domain (O'Sullivan et al., 2012). Intercellular homophilic Flrt dimerization, or heterophilic Flrt/Lphn binding, are adhesive and promote outgrowth. However, context is important, as Unc5, the Netrin receptor, can also bind Flrt and this interaction leads to cell repulsion (Jackson et al., 2016; Lu et al., 2015).

Due to the evidence of Lphn in the adhesive activity of Flrt, we examined co-expression of *Flrt* and *Lphn* during NTC. We observed that *Flrt* and *Lphn* are expressed in non-overlapping domains within the closing neural plate (Figure 2.5). One striking feature of *Lphn* expression is its dynamic nature. At the start of neurulation (stage 13), before the neural folds have begun to close, *Lphn* is expressed laterally and posteriorly to the stripe of *Flrt* expressing cells (Figure 2.5A). As the neural folds begin to close, progressing from posterior to anterior

(stage 15), the expression of *Lphn* shifts anteriorly. At this stage, *Lphn* is expressed along the lateral edges of neural folds, surrounding *Flrt* expression. This distribution is consistent with published *in situs* for *Lphn* (Dardaillon et al., 2020). As neural tube closure progresses (st.16), posterior neural tube expression of *Lphn* is lost, but expression remains in the anterior-most region where the neural folds are still closing and continues to surround the domain of *Flrt* expression (Figure 2.5A). In addition to the neural plate expression, *Lphn* was also observed in the mesenchyme (yellow arrowhead). This dynamic expression occurs over the course of less than two hours at 18°C, from late gastrula stage (st.13) at about 5.9 hours post-fertilization to late neurula stage (st.16) at about 7.4 hours post fertilization (Figure 2.5A). The expression of *Lphn* appears to be at the neural-epidermal boundary of the neural folds. To determine whether either the *Flrt* or *Lphn* expression domains extend into epidermal tissue, we performed *Flrt* or *Lphn in situs* along with the pan-neural marker *ETR-1*. *Flrt* mRNA is present in the center of the neural tube and overlaps completely with *ETR-1* (Figure 2.5B), as does the neural expression domain of *Lphn* (Figure 2.5C). Taken together this indicates that *Flrt* and *Lphn* are expressed in opposing domains of the developing neural tube.

**NTC defects in embryos with gain or loss of *Flrt* complex genes**

Because both tissue separation and adhesion are essential for NTC, gene products identified in our RNAseq screen could play a role in either, or both processes. This is particularly true for Flrt, which can act as a cell adhesion

molecule through homophilic binding or heterophilic binding with Lphn, or as a repulsive ligand to Netrin/Unc5 receptors (Seiradake et al., 2014). Due to this dual function, we hypothesize that not only overexpression, but also under-expression of Flrt could lead to abnormal adhesion/repulsion during neural tube closure and an OB phenotype. Accordingly, we assessed both gain of function (*i.e.*, overexpression) and loss of function (*i.e.*, CRISPR/Cas9 gene editing). To assess gain of function, *Flrt* cDNA was expressed in transiently-transfected embryos by electroporation (Zeller, 2018) using the promoter from the anterior neural plate gene *OTX* (plasmid OTX>*Flrt*) along with GFP expressed under control of the ETR-1 promoter (plasmid ETR-1>GFP) to mark the CNS. OTX, a homeobox transcription factor, is expressed first early in the 32-cell embryo (Hudson and Lemaire, 2001). Once gastrulation is initiated, *OTX* is strongly upregulated in neural plate precursors, and by the tailbud stage is expressed in the anterior brain (Hudson and Lemaire, 2001). Approximately half of embryos electroporated with the OTX>*Flrt* construct had an OB phenotype, while OB was rare in embryos transfected with the control plasmid (OTX >RFP) (50.1%, versus 5.5% in controls, Figure 2.6A; ***$p < 0.00001$, Fisher's exact test). This phenotype, like that of *bug* mutants, is characterized by ETR-1>GFP positive neural tissue protruding from the larval head (Figure 2.6B, white arrow). Representative control embryos have a closed neural tube with no ectopic ETR-1>RFP positive tissue (Figure 2.6C).

To examine the loss of function phenotype for Flrt, we used the CRISPR/Cas9 system to edit the *Flrt* as well as *Lphn* gene in *C. robusta*

embryos. Embryos were electroporated with U6>sgRNA and eF1-alpha > Cas9 constructs (see above) and grown to the hatched larva stage (24 hours at 18◦C) when they were scored for the OB phenotype. *Flrt* and *Lphn* sgRNA electroporated animals had a higher percentage of OB than control embryos (8.9% and 10.8% respectively, versus 1.2% for control) (Figure 2.6D; *** $p < 0.00001$, * $p < 0.05$, Fisher's Exact Test). To investigate *Lphn* and *Flrt* CRISPR/Cas9 results further, we isolated two genomic DNA pools from each sample, one pool with OB phenotype, and the other with CB phenotype. Fragments surrounding the *Flrt* and *Lphn* sgRNA targets were then PCR amplified and Sanger sequenced. With the genomic DNA pools, genomic editing is evident as disorganized sequence starting at the target of the sgRNA in both the *Flrt* and *Lphn* OB pools (Figure 2.6E, arrows). By contrast, this was not observed in either of the CB pools. This result is consistent with genome editing of *Flrt* and *Lphn* leading to OB phenotypes. We also assessed CRISPR/Cas9 gene editing of *Sel*. Embryos electroporated for *Sel* sgRNA had a significantly higher percentage of OB (4.5%, $p< 0.05$, Fisher's Exact Test) than embryos electroporated with the control sgRNA (1.2%) (Figure 2.6D). Loss of either *Sel* or *Flrt*, along with its binding partner *Lphn*, lead to the OB present in *bug* mutants indicating they play a causative role in this phenotype and likely have an important role in NTC.

## E. Discussion

RNAseq analysis of *bug* mutants has revealed misregulation of a number of transcripts. Our analyses point to the cell adhesion molecules *Sel* and *Flrt* as playing roles in NTC. Both these genes are upregulated in *bug* mutants, and CRISPR/Cas9 mediated gene editing phenocopies the *bug* mutant. *Sel* in particular was the most highly upregulated transcript found in the *C. robusta bug* mutant (Supplemental Table 2.1). Selectins are type-1 membrane glycoprotein members of the C-type Lectin family (Nagaoka et al., 2000; Yukami et al., 2007). In *Drosophila* embryos, Sel mutants (*furrowed*) are defective in the planar cell polarity (PCP) pathway, in part through defects in homophilic cell adhesion (Chin and Mlodzik, 2013). The PCP pathway has been shown to be important for neural tube closure in vertebrates in the generation of polarized actomyosin contractions driving the formation of the neural folds (Heisenberg and Bellaïche, 2013; Nishimura et al., 2012). However, the *bug* mutants show no defects in neural fold formation (Abdul-Wajid et al., 2015). Moreover the *aimless* mutant of *Ciona*, which has a null mutation in the PCP component *prickle*, is able to complete NTC despite a complete disruption of convergent extension in the notochord, suggesting no role for the PCP pathway in *Ciona* NTC (Jiang et al., 2005). Consistent with this, the mechanism of action of the Selectin family in vertebrates appears to be highly divergent from that in *Drosophila*. In vertebrates the best characterized role of Sel is in the tethering of leukocytes on endothelial

cells through cell adhesion involving cell-surface markers (McEver, 2002). We find that *Sel* is highly expressed in the closing neural tube and targeting the *Sel* gene with CRISPR/Cas9 results in open neural tubes. Moreover, *Sel* is upregulated in larvae that display an open brain phenotype from knockout of other cell adhesion factors that function in NTC. Taken together, these results are consistent with a role for Sel in NTC and it is likely that its role is one involving its adhesive properties.

The biological activity of Flrt is complex, and in different contexts can promote or inhibit cell adhesion. In *Xenopus*, Flrt promotes de-adhesion during gastrulation (Ogata et al., 2007), while in the mouse Flrt appears to promote cell adhesion as embryos carrying null alleles are defective in ventral closure, headfold fusion and definitive endoderm migration (Maretto et al., 2008). Additionally, Flrt has well-known roles in neurite outgrowth and synapse formation (Kiryushko et al., 2004). The transmembrane protein Flrt forms part of a large multiprotein complex of varying compositions, depending on the context, and one of the best described binding partners of the Flrt complex is Lphn (Jackson et al., 2015; del Toro et al., 2020). Our results from CRISPR/Cas9, targeting both *Flrt* and *Lphn,* show that both are essential for *Ciona* NTC. Moreover, their expression domains are non-overlapping, similar to what is seen in neurite outgrowth, with *Flrt* being medial and *Lphn* being lateral within the neural plate (Figure 2.4). It is possible that additional factors are involved, such as Unc5 which plays a role in repulsion during neurite outgrowth (Jackson et al., 2016; Lu et al., 2015). Interestingly, our findings point to the potential reuse of

morphogenetic mechanisms for NTC and neurite outgrowth, suggesting that the same interactions that promote stabilization of synapses may also act in the neural tube to promote closure. Additionally NCAM, which plays a role in NTC, also has a well-known role in neurite outgrowth (Hansen et al., 2008). The distinct peak in expression of Flrt during neurulation, in combination with the expression of Lphn during the same stages, points to a role for these molecules in NTC. While its temporal expression suggests it may not be acting in neurite outgrowth during larval development, it is unknown whether Flrt is acting in this process at later stages in *Ciona*.

The expression pattern for *Lphn* is highly dynamic, moving from the posterior to the anterior end of the embryo as the neural tube closes (Figure 2.4A). While the *Flrt* expression domain is restricted to the anterior portion of the neural tube and likely functions in anterior closure, *Lphn* is transiently expressed along the entirety of the neural tube, possibly suggesting a more general role in NTC. However, when knocked out in wild-type *Ciona,* larvae only exhibit defects anteriorly, indicating it may also be playing a more specific role in anterior NTC. Given this, its role during early morphogenesis may be dependent on its interactions with Flrt. The expression patterns of the two molecules support this hypothesis, but future work needs to be done to assess their possible functional interactions. Due to transient expression of both *Flrt* and *Lphn* during NTC, and *Flrt* downregulation at the end of NTC (Figure 2.2C), it is likely they participate in molecular recognition events and promotion of neural fold adhesion, rather than

in the long-term stabilization of this interaction. In fact, other cell molecules, including N-cadherin and NCAM, are better suited to the stable adhesion.

In summary, the RNAseq analysis of the *bug* mutant has led to the identification of a number of differentially expressed genes. This study focused on the cell adhesion molecules Sel and Flrt, both of which are aberrantly upregulated in the *bug* mutant. It is of particular interest that at least three of these molecules, both Sel and Flrt (described here, Figure 2.2C,D) as well as EphrinA-d (described previously (Abdul-Wajid et al., 2015)), experience peaks of expression during neurulation in wild-type embryos. Upregulation of these transcripts in our mutants could be the result of a failure to downregulate following completion of NTC. The causative mutation in *bug* mutants stems from aberrations in the *Cav3* gene, which may act in a regulatory step at the end of NTC, turning off certain transcripts required for NTC, and possibly turning on others that are required for the next developmental process, as is indicated by the large number of downregulated genes in *bug* mutants (Supplemental Table 2.1). However, the direct mechanism between this Cav3 (a T-type calcium channel) and transcript regulation is not clear and would be an informative focus for future research. These new findings, with the addition of Sel and Flrt, add to the complexity of models of chordate NTC and are steps towards a more comprehensive understanding of this process.

## F. Figures

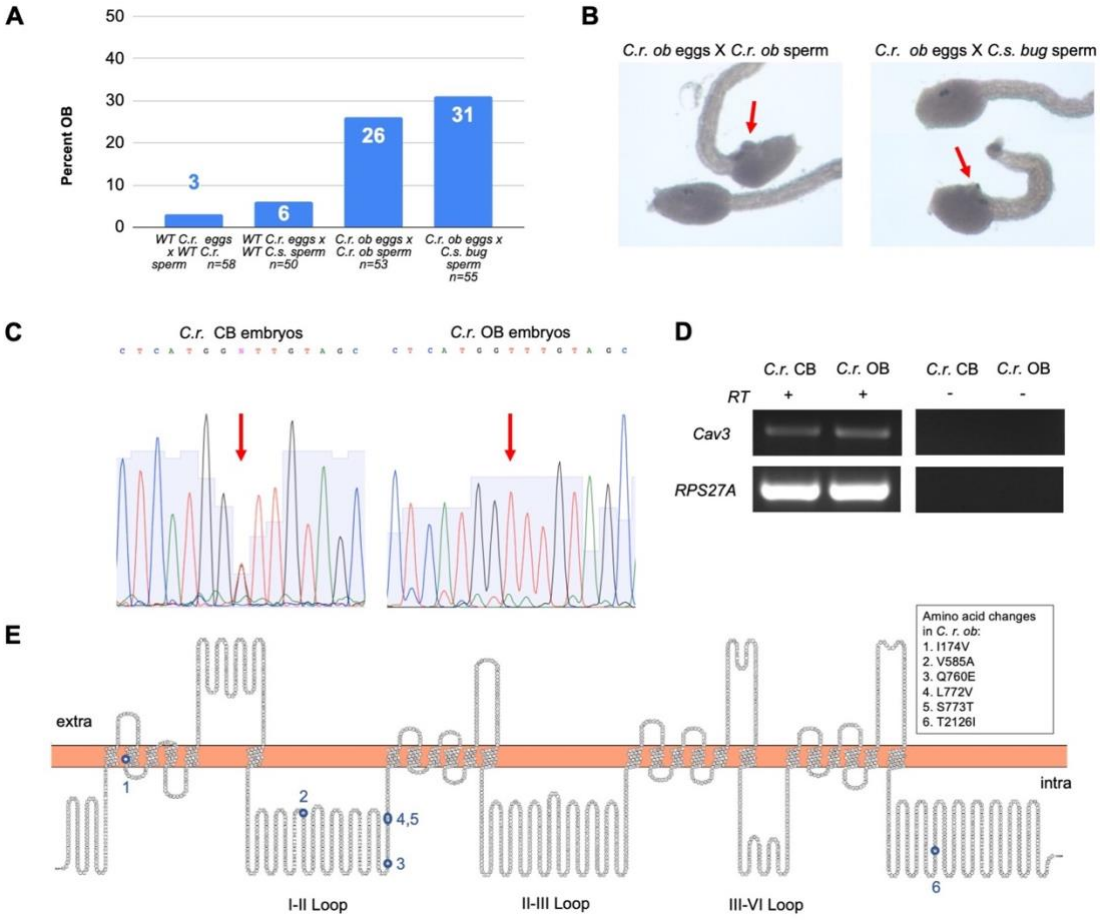


**Figure 2.1.** *Ciona robusta* open brain mutant (*ob*). **A**. Complementation test between *C. robusta ob* (*C.r. ob*) and *C. savignyi bug* (*C.s. bug*) mutants. Open brain (OB) phenotypes were observed from crosses of *C.r. ob* eggs to *C.r. ob* sperm, and from crosses of *C.r. ob* eggs to *C.s. bug* sperm at frequencies of 26% and 31%, respectively. **B**. Representative examples of OB (red arrow) and closed brain (CB) phenotypes. **C**. Linkage analysis of *C.r. ob* to the *Cav3* locus using progeny of crossed *C.r. ob* heterozygous adults. Red arrows indicate a

single nucleotide polymorphism that is present in CB larvae, but that resolves to a single nucleotide in OB siblings. **D**. Expression of Cav3 by RT-PCR in CB and OB *C.r. ob* larvae. **E**. Structure prediction of *C. robusta* Cav3. Amino acid changes found in the *ob* allele are indicated in the sequence. Multiple amino acid substitutions were observed in the I-II loop. Structure manually plotted and image generated using Protter (Omasits et al., 2014).

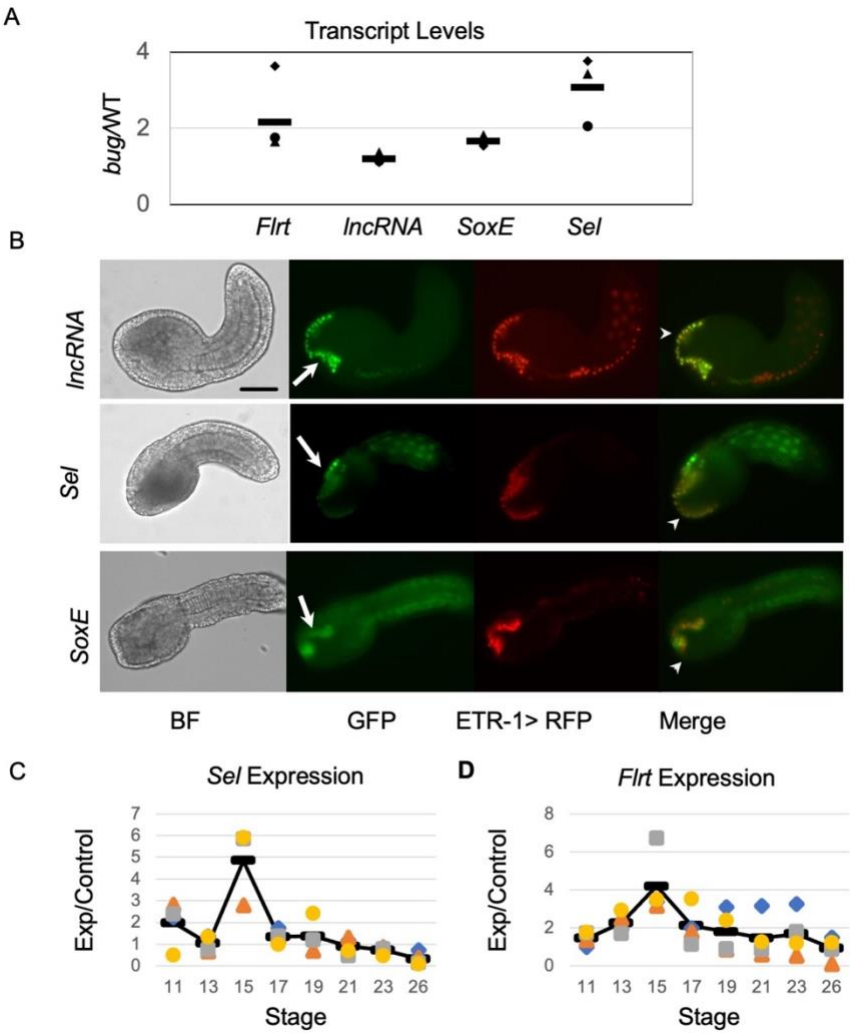


**Figure 2.2**. Upregulated genes found in RNAseq analysis are expressed in neural tissue. **A**. Validation of select transcripts identified as differentially expressed by RNAseq. Transcript levels were determined by RT-PCR. Results show the average level of transcript in *bug* compared to the wild type larvae (line) from three separate replicates. **B**. GFP from *long non-coding RNA* (*lncRNA*), *Selectin* (*Sel*), and *SoxE* promoter constructs is visible in the brain (arrows) and in the palps (arrow heads). Scale bar = 50 µm. **C** and **D**. Transcript levels determined by RT-PCR of *Sel* (C) and *Flrt* in wild-type embryos across several stages of development in four separate samples.

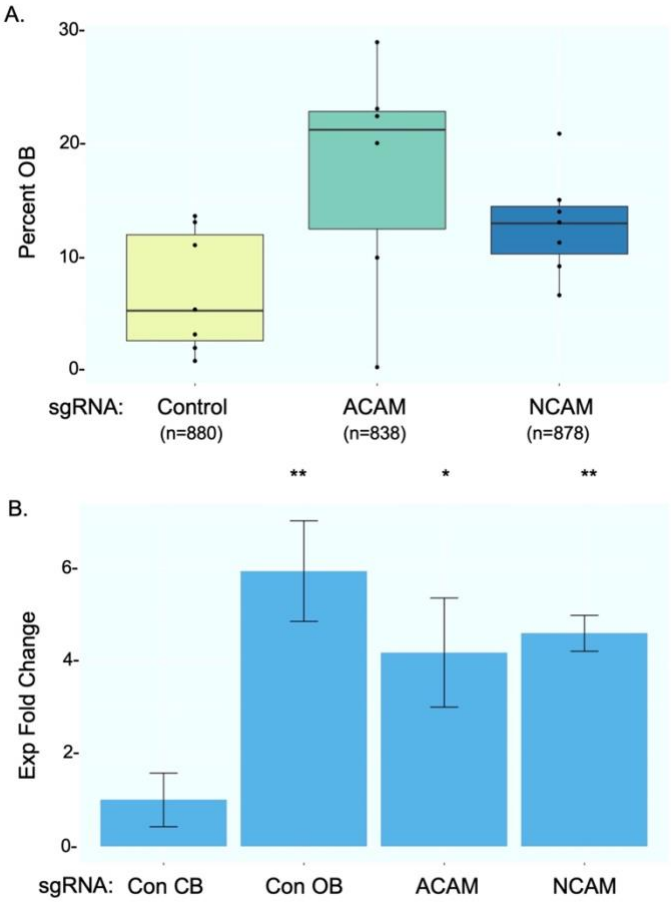


**Figure 2.3.** Disruption of multiple NTC pathways leads to an increase in *Sel* expression. **A.** Percent open brain (OB) phenotype in larva resulting from CRISPR/Cas9 gene editing with the indicated sgRNA. $P > 0.00001$, Fisher Exact test. **B.** Expression fold change of *Sel* mRNA in embryos subjected to CRISPR/Cas9 genome editing with the indicated sgRNA. Each point is 3 replicates of a separate CRISPR/Cas9 experiment. Con CB: embryos electroporated with the control sgRNA that exhibited closed brains. Con OB: control sgRNA treated embryos that had OB due to spontaneous neural tube defects in dechorionated embryos *$p < 0.05$, **$p < 0.001$ T-test (based on dCT values).

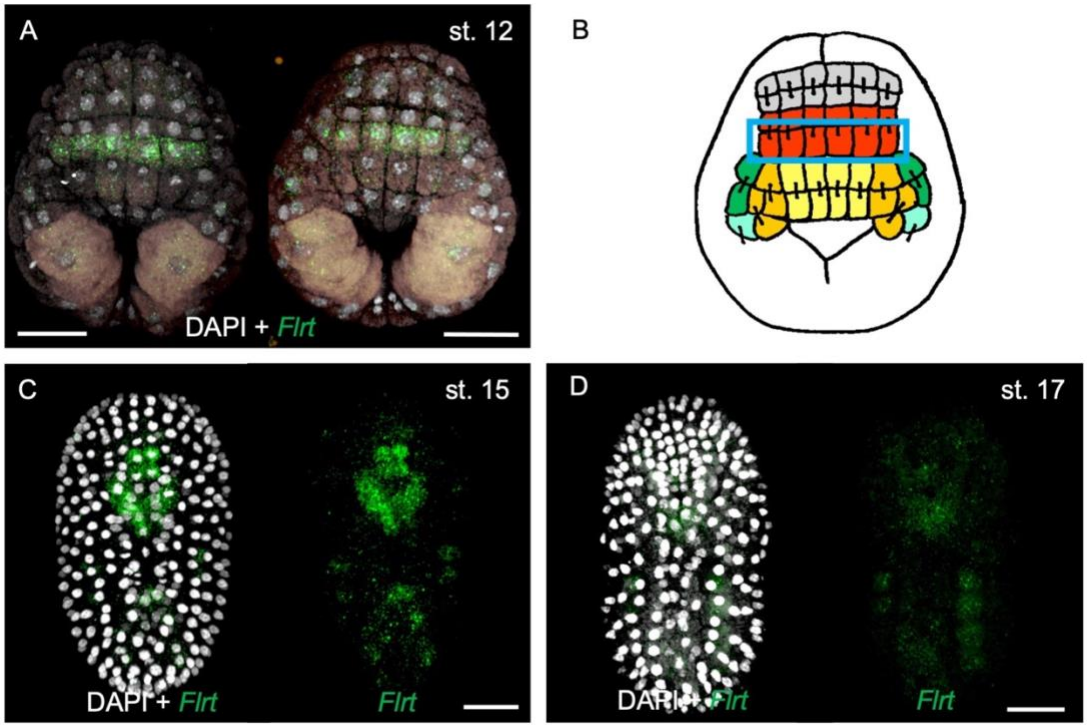


**Figure 2.4.** Time course of FLRT expression in neurulation. *Flrt* expression is green, while nuclei stained with DAPI are shown as white. **A**. Mid-gastrula stage embryos showing a distinct stripe of *Flrt* expression in the neural plate. **B**. Cartoon of the neural plate during mid gastrula. Blue box indicates the *Flrt*-expressing cells (adapted from (Hudson, 2016)). **C**. Mid-neurula stage embryo showing *Flrt* expression. **D.** Initial tailbud stage embryo showing *Flrt* signal in the neural tube as closure is nearing completion. Scale bars = 30 µm.

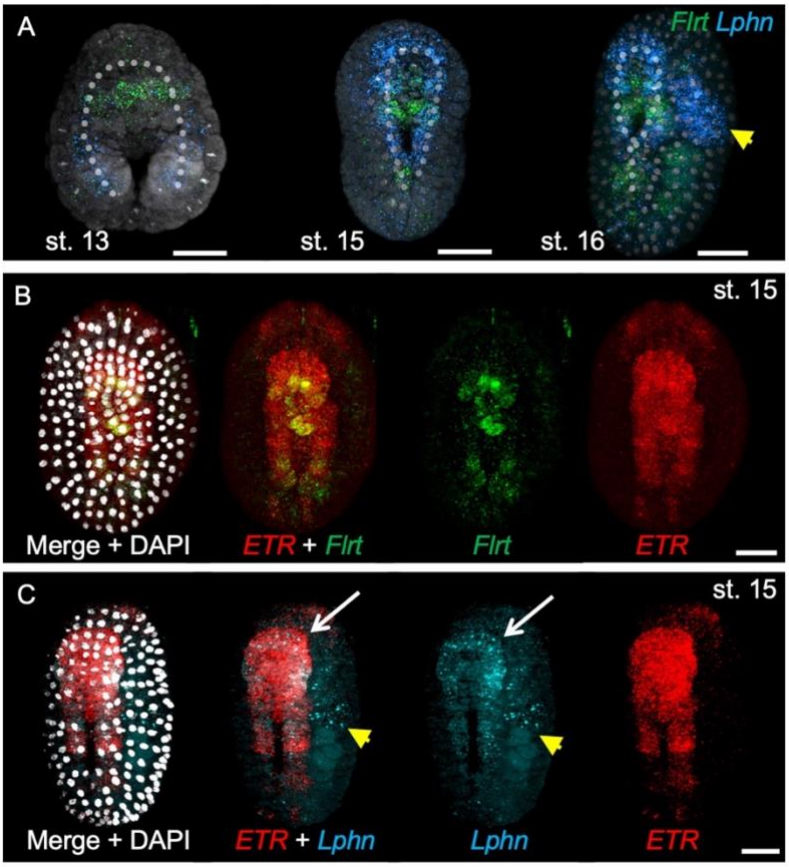


**Figure 2.5.** *Lphn* and *Flrt* are expressed in opposing domains within the closing neural tube. Hybridization Chain Reaction (HCR) *in situs* showing localization of *Flrt* (green) and *Lphn* (blue) during neural tube closure. **A.** Progression of *Flrt* and *Lphn* localization across several stages of neurulation. White dotted lines show the location of the closing neural folds. Mesenchymal expression of *Lphn* designated by the yellow arrowhead. **B**. Mid-neurula stage embryos showing *Flrt* co-localization with ETR (red). Nuclei are stained with DAPI (white). **C.** Mid-neurula stage embryos showing *Lphn* co-localization with *ETR* (white arrows). Mesenchymal expression of *Lphn* designated by yellow arrowheads. Nuclei are stained with DAPI (white). Scale bars = 30 µm.

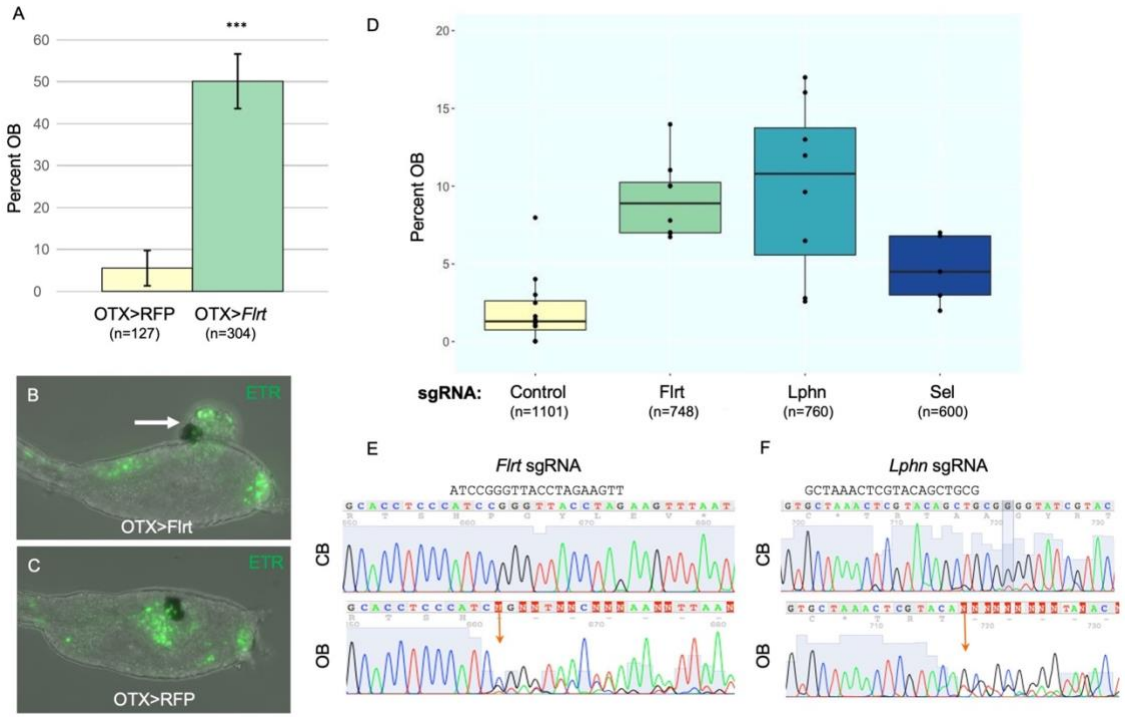


**Figure 2.6.** Overexpression and CRISPR/Cas9 gene editing of *Flrt* results in open brain phenotypes. **A.** Percentage of open brain (OB) phenotype observed in wild type embryos electroporated with either a *Flrt* cDNA expression construct (OTX>Flrt), or an RFP cDNA control expression construct (OTX>RFP), driven by the brain OTX promoter. Results are shown as the average percentage of OB phenotype from three independent trials. Error bars represent the standard deviation. Asterisks indicate significance, $p < 0.00001$, Fisher's exact test. **B** and **C**. *Flrt* overexpression in *C. robusta* embryos, but not RFP overexpression phenocopies the *bug* mutant. B. White arrow indicates the OB. The nervous system is labeled with ETR > H2B:GFP. C. Control embryo expressing ETR > H2B:GFP has a closed brain (CB). **D**. Percent OB in larva resulting from CRISPR/Cas9 with the indicated sgRNA. Each dot is an independent

replicate. ***p < 0.00001, * p < 0.05, Fisher's exact test. **E** and **F**. DNA isolated from pooled embryos with an OB or a CB phenotype following knockout with sgRNA targeted to *Flrt* or *Lphn* was PCR amplified and sequenced around the sgRNA site. In DNA from animals with an OB phenotype, but not DNA from animals with a CB, evidence of imprecise repair of genome editing is present in overlapping peaks in Sanger sequencing results. Red arrows indicate the start of divergent sequences.

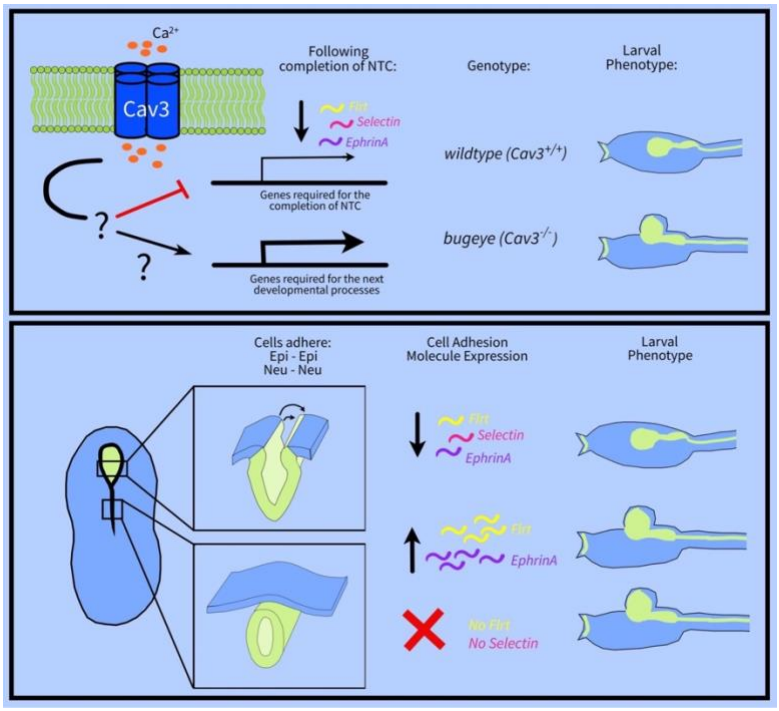


**Figure 2.7.** Graphical Abstract/Model – (Top) We hypothesize that signaling through Cav3 may act as a mechanical developmental checkpoint that monitors the progress of neural tube closure and upon completion works to downregulated genes required for the completion of NTC, and possibly upregulated genes required for the next developmental processes. *Cav3* mutant larvae (*bugeye*) fail to properly close the neural tube and display on open brain phenotype. (Bottom) Following neurulation, expression of several cell adhesion molecules is downregulated. When these cell adhesion molecules are either aberrantly upregulated or knocked out altogether, larvae display an open brain phenotype similar to that of *bugeye* mutants. We hypothesize that because the final stages of NTC involve both formation and release of cell-cell junctions, that a delicate balance of cell adhesion proteins must be maintained and that either too little or too high levels of these proteins can interfere with the sealing of the neural tube.

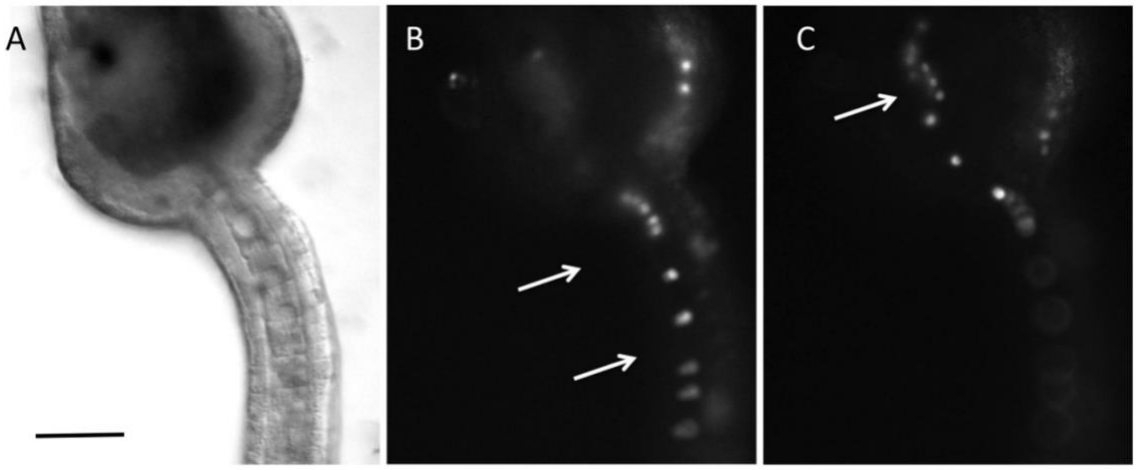


**Supplemental Figure 2.1. A.** Bright field view of late-tailbud embryo. B and C. GFP expression from an embryo electroporated with an *Ependymin* promoter-GFP construct. Two different focal planes are shown. Expression is in the nerve cord (B) and brain (C, arrows). Scale bar = 30 µm.

## G. Tables

**Supplemental Table 2.1:** List of differentially expressed genes between mutant (*bugeye*) and wild-type larvae for both *C. savignyi* and *C. robusta*. Listed are the gene identification number (Ensembl), fold change (shown as logFC), false discovery rate (FDR), and when available the best human hit resulting from a BLAST (NCBI) search. The gene model ID as listed in the ascidian database Aniseed is also given, when available, for differentially expressed genes in *C. robusta.*

***C. savignyi* upregulated genes**

| Gene | logFC | FDR | Best Human Hit |
|---|---|---|---|
| ENSCSAVG00000003155 | 11.883119 | 2.32E-43 | FLRT |
| ENSCSAVG00000000912 | 10.527853 | 5.63E-09 | CBR1/3 |
| ENSCSAVG00000001384 | 1.451407 | 2.80E-02 | |
| ENSCSAVG00000001143 | 1.209009 | 2.80E-02 | |
| ENSCSAVG00000007345 | 1.103210 | 1.00E-03 | ACRO |

***C. savignyi* downregulated genes**

| Gene | logFC | FDR | Best Human Hit |
|---|---|---|---|
| ENSCSAVG00000006120 | -9.24 | 2.56E-13 | NTAQ1 |
| ENSCSAVG00000011320 | -8.80 | 1.91E-05 | |
| ENSCSAVG00000002864 | -8.67 | 5.93E-10 | ICE2 |
| ENSCSAVG00000011387 | -8.42 | 2.84E-02 | SH3BG; SH3L1/L2 |
| ENSCSAVG00000006581 | -7.27 | 3.56E-02 | |
| ENSCSAVG00000008044 | -7.01 | 1.81E-03 | AURKA |
| ENSCSAVG00000002112 | -6.83 | 2.11E-02 | Tim10/DDP |
| ENSCSAVG00000011200 | -6.54 | 4.99E-02 | ASGL1 |
| ENSCSAVG00000006895 | -5.82 | 1.39E-04 | |
| ENSCSAVG00000001882 | -5.62 | 4.93E-02 | FBXW7 |
| ENSCSAVG00000006880 | -5.52 | 2.84E-02 | |
| ENSCSAVG00000009968 | -4.79 | 3.96E-02 | |
| ENSCSAVG00000003400 | -4.10 | 4.45E-03 | |
| ENSCSAVG00000011667 | -3.86 | 2.13E-02 | |
| ENSCSAVG00000006175 | -3.72 | 1.39E-04 | NAT-3 |
| ENSCSAVG00000004011 | -2.24 | 2.80E-02 | R-PTP-N2 |

| | | | |
|---|---|---|---|
| ENSCSAVG00000005413 | -1.61 | 6.93E-07 | MCFD2 |
| ENSCSAVG00000006951 | -1.10 | 1.07E-02 | CHST3/4 |
| ENSCSAVG00000003702 | -1.08 | 2.84E-02 | VPS36 |
| ENSCSAVG00000009489 | -1.07 | 3.14E-03 | B3GN2/6/7 |
| ENSCSAVG00000004117 | -1.04 | 2.37E-02 | VRK |
| ENSCSAVG00000004578 | -0.80 | 3.41E-02 | SMD1 |

***C. robusta* upregulated genes**

| Gene | logFC | FDR | Gene Model ID | Best Human Hit |
|---|---|---|---|---|
| ENSCING00000004297 | 4.45 | 3.88E-07 | KH.C1.372 | SELL |
| ENSCING00000018048 | 3.85 | 2.15E-02 | | |
| ENSCING00000023102 | 3.49 | 1.09E-02 | KH.S1120.3 | |
| ENSCING00000025046 | 2.30 | 1.88E-05 | KH.S1120.4 | |
| ENSCING00000006967 | 2.25 | 2.48E-02 | KH.C1.260 | IL17B/C/D |
| ENSCING00000021930 | 2.14 | 9.84E-04 | KH.C6.228 | SPI1/B/C |
| ENSCING00000004648 | 2.09 | 7.11E-06 | KH.C10.322 | CDKAL |
| ENSCING00000015638 | 1.93 | 2.09E-03 | KH.L134.23 | IL17B/C/D |
| ENSCING00000019332 | 1.92 | 9.79E-02 | KH.C6.275 | |
| ENSCING00000023653 | 1.67 | 1.22E-02 | KH.S529.5 | |
| ENSCING00000022137 | 1.59 | 7.11E-06 | KH.L172.16 | EGR-1/2/3 |
| ENSCING00000025112 | 1.51 | 3.74E-02 | KH.C6.281 | FGFR1/2/3 |
| ENSCING00000023989 | 1.46 | 1.55E-03 | KH.L119.17 | HIPK2 |
| ENSCING00000018897 | 1.35 | 6.21E-03 | KH.C6.169 | |
| ENSCING00000008770 | 1.32 | 2.84E-03 | KH.L154.36 | CYP4F2/22/3 |
| ENSCING00000005686 | 1.28 | 5.08E-10 | KH.L46.6 | HSPA1A/B |
| ENSCING00000003515 | 1.21 | 3.17E-04 | KH.C1.659 | |
| ENSCING00000012282 | 1.19 | 6.40E-02 | | |
| ENSCING00000019105 | 1.19 | 4.50E-03 | KH.S753.2 | ADGRB3 |
| ENSCING00000001019 | 1.09 | 3.17E-04 | KH.L154.42 | SOX8/9/10 |
| ENSCING00000025117 | 1.04 | 3.90E-02 | KH.C2.151 | PAICS |
| ENSCING00000018362 | 0.99 | 3.43E-03 | KH.C6.264 | |
| ENSCING00000004419 | 0.99 | 4.61E-02 | KH.C2.703 | BMP1 |
| ENSCING00000001621 | 0.93 | 7.30E-10 | KH.C1.90 | SLC25A21/33/36 |
| ENSCING00000016222 | 0.91 | 3.81E-06 | KH.C2.1055 | PLA2G1B/2A/2E |
| ENSCING00000022351 | 0.90 | 9.18E-02 | KH.C11.17 | BMT2 |
| ENSCING00000024466 | 0.86 | 3.81E-05 | KH.C11.667 | LncRNA |

***C. robusta* downregulated genes**

| Gene | logFC | FDR | Gene Model ID | Best Human Hit |
|---|---|---|---|---|
| ENSCING00000023719 | -4.13 | 1.54E-19 | KH.C6.253 | ZN112 |

| | | | | |
|---|---|---|---|---|
| ENSCING00000021537 | -3.16 | 9.55E-02 | KH.C4.743 | |
| ENSCING00000022601 | -2.96 | 7.80E-03 | KH.C11.398 | EPDR1 |
| ENSCING00000025206 | -2.64 | 1.09E-04 | | ND4 |
| ENSCING00000014977 | -2.58 | 2.84E-03 | KH.L116.3 | ACSM4 |
| ENSCING00000018002 | -2.34 | 6.21E-02 | KH.C6.126 | KLHL10/12/20 |
| ENSCING00000019996 | -1.99 | 3.73E-05 | KH.C6.260 | CYP4 |
| ENSCING00000005852 | -1.97 | 3.43E-03 | | JAG2L |
| ENSCING00000024442 | -1.90 | 1.41E-13 | KH.C7.558 | |
| ENSCING00000025215 | -1.81 | 1.61E-02 | | ND3 |
| ENSCING00000010806 | -1.73 | 4.40E-04 | KH.C6.134 | PTPRA |
| ENSCING00000020050 | -1.70 | 4.82E-02 | KH.L90.5 | DUSP15/9/22 |
| ENSCING00000020024 | -1.50 | 2.55E-02 | KH.S423.8 | S22A1/3/5 |
| ENSCING00000016270 | -1.50 | 5.14E-02 | KH.S423.8 | S22A1/3/5 |
| ENSCING00000007176 | -1.46 | 4.12E-13 | KH.C7.729 | CO6A6 |
| ENSCING00000019890 | -1.29 | 5.92E-02 | | |
| ENSCING00000020879 | -1.26 | 7.20E-02 | KH.C11.12 | ARSB/I/J |
| ENSCING00000022994 | -1.19 | 9.84E-04 | | |
| ENSCING00000010470 | -1.12 | 1.61E-02 | KH.L20.5 | GSTA1/2/3/4 |
| ENSCING00000011763 | -1.10 | 1.59E-02 | KH.C3.438 | CSMD3 |
| ENSCING00000014847 | -1.03 | 4.50E-03 | KH.C6.28 | CRLD2 |
| ENSCING00000002439 | -1.01 | 4.64E-06 | KH.L59.3 | CRIS2 |
| ENSCING00000020952 | -1.00 | 8.29E-02 | KH.C7.471 | |
| ENSCING00000024469 | -1.00 | 1.79E-03 | KH.C6.18 | CCDC58 |
| ENSCING00000020909 | -0.91 | 2.13E-05 | KH.S728.2 | CDKAL |
| ENSCING00000020117 | -0.79 | 8.29E-02 | KH.C12.549 | ACAN |
| ENSCING00000016436 | -0.79 | 8.29E-02 | KH.S831 | |
| ENSCING00000015064 | -0.75 | 5.86E-04 | KH.L59.3 | CRIS2 |
| ENSCING00000020806 | -0.74 | 9.55E-02 | KH.C6.86 | ARF1/3/5 |
| ENSCING00000022945 | -0.73 | 7.74E-02 | KH.C6.145 | CHRD/L1/L2 |
| ENSCING00000016188 | -0.68 | 3.90E-02 | KH.C6.176 | NHRF3/4 |
| ENSCING00000004446 | -0.65 | 2.62E-02 | KH.C6.94 | TP53I11 |
| ENSCING00000004066 | -0.65 | 2.00E-02 | KH.C6.234 | CP4F2/3/8 |
| ENSCING00000007740 | -0.64 | 2.72E-03 | KH.C10.68 | LOX5 |
| ENSCING00000024083 | -0.58 | 4.82E-02 | KH.C2.373 | |
| ENSCING00000001585 | -0.55 | 2.56E-02 | KH.L20.47 | BDH2 |
| ENSCING00000002614 | -0.50 | 6.21E-02 | KH.C1.326 | AMOL1 |
| ENSCING00000019439 | -0.50 | 7.20E-02 | KH.L27.2 | |
| ENSCING00000002641 | -0.49 | 6.21E-02 | KH.C9.692 | GABRR1/2/3 |
| ENSCING00000006444 | -0.46 | 9.79E-02 | KH.C3.410 | PEAK1 |
| ENSCING00000023171 | -0.46 | 5.81E-01 | | |

**Supplementary Table 2.2**. Primer sequences, related to experimental procedures.

| NAME | SEQUENCE | GENE MODEL ID |
|---|---|---|
| **Linkage analysis primers** | | |
| Cav3 F | TTGTCCAAAATCGTGGCATA | KH.C6.65 |
| Cav3 R | TAAAAGTCGCCACGTTGTCC | |
| | | |
| **Cav3 cDNA primers** | | |
| Section 1F | GCGAACCCATATCCTTTTCA | |
| Section 1R | TGCAATTACATCTGCTTTTGTTT | |
| Section 2F | CAGAACAAGAAATTGAAATCAAAA | |
| Section 2R | CTCACGAATTGTGTCCTTCA | |
| Section 3F | CCGGTCACTGCTGGAAAC | |
| Section 3R | GCTAACCAAATGATAGGCCGTAA | |
| Internal Sequencing primer F1 | AGCGACTCAGTTCTCAGAAACA | |
| Internal Sequencing primer F2 | ATACACTAAGTATGGGCATTGAACA | |
| Internal Sequencing primer F3 | TACAATGTTTTCGACGCACTT | |
| Internal Sequencing primer R1 | CTCGTTTGATCTCGACTGATTC | |
| | | |
| **RT-PCR primers** | | |
| Cav3 RT | AGGACAAGGTGCAACAAACTG | KH.C6.65 |
| | TGTGTGCCTGCTGCTATTTC | |
| RPS27A RT | CACCCTTGAGGTTGAAGCAT | KH.C10.239 |
| | GGTTCTCAGGTTTGAACACG | |
| Flrt RT | TGAACGACGCTTCATTTCAG | KH.C6.163 |
| | TCGCCTCGTATCGGTATTTC | |
| lncRNA | TCGCTTGAGTGGTGGTAGAA | KH.C11.667 |
| | TTCCCTCTTCAGCCTTTTGA | |
| SoxE | GAACACTGGCTCATCTGCAA | KH.L154.42 |
| | CCCGAGTGTTTTGCTGAGTT | |
| Sel | ACGAGGCAGAGAACCACTGT | KH.C1.372 |
| | CGAACGACAAAGCCACATTA | |
| | | |
| **Expression construct primers** | | |
| SoxE | CGTAAACATAAGGCGGGTCG | KH.L154.42 |
| | TATCGTAGCGACGTGATGTTG | |
| Sel | TCAAATATAGGCGCCCGTAAAC | KH.C1.372 |

| | | |
|---|---|---|
| | TGTGTAATTTTGCAAAAAAAACTAAC | |
| lncRNA | AACCTTCGCCTCCCAAAGAA | KH.C11.667 |
| | CCGAGTTCCAGCACGTTGGC | |
| Ependymin | GCGTTTTACAGCAGCCAGTA | KH.C11.398 |
| | TGTTGTAAATGTATCTGTTTAAGTCTTATACC | |
| Flrt cDNA | ATGATTAAGCGTTTTTGCTTCATTGTTG | KH.C6.163 |
| | AACGAAAAGCCCAGAGTCGTG | |
| **sgRNA sequence** | | |
| ACAM A | GCCGTTCTCCGCAGACTCCG | KH.C4.506 |
| ACAM B | GTTGAGAGAGCGACGAACGC | |
| NCAM A | GCTGTTATATGCCAGGTGTC | KH.C10.260 |
| NCAM B | GGGTAATCCTCCACCAAGTG | |
| Sel A | GGTGTCTCTGTTGCGCGAACG | KH.C1.372 |
| Sel B | GGGGGAGAACTTCATTACCAC | |
| CONTROL | GCTTTGCTACGATCTACATT | |
| Lphn A | CTTTGCTACGATCTACATT | KH.C5.597 |
| Lphn B | GCTAAACTCGTACAGCTGCG | |
| Flrt A | GACTTCTAGGTAACCCGGAT | KH.C6.163 |
| **Primers to check for gene editing** | | |
| Flrt | GCTCAAGACGGAAAAGCTCA | KH.C6.163 |
| | TGTGATATTACCCGGCAGCT | |
| Lphn | TCCTCAGGACTTCGCTC | KH.C5.597 |
| | AAACAGTTGCCGCTACCTG | |
| **RT-qPCR primers** | | |
| Actin | GTACATGGCGGGGGTGTTG | KH.L154 |
| | AACTCCGTGTCGCACCAGAA | |
| RSP27A | GCAAGCTTGACTTTGACACG | KH.C10.239 |
| | CACCCTTGAGGTTGAAGCAT | |
| Sel | ATGGACATCACCCCAGCACC | KH.C1.372 |
| | TGCATCAGGTGTATTGGCGGA | |

## III. Pharmacological inhibition of Cav3 and mechanical disruption of NTC are alternative methods for producing the open brain phenotype.

### A. Abstract

The appearance of the open brain phenotype in *bugeye* mutants does not occur until well after neurulation, despite the fact that inhibiting Cav3 during NTC is the optimal time for producing the phenotype. Additionally, homozygous *bugeye* mutants fail to undergo metamorphosis into adult *Ciona* making it necessary to propagate them as heterozygotes. As a result, analysis of the neurula stage mutant is extremely difficult. To provide a robust way of producing the open brain phenotype, I used several different drugs to inhibit T-type calcium channels to varying degrees of success. One of the most successful treatments was exposing neurulating embryos to $ZnCl_2$ on the embryos during neurulation. However, transcriptional analysis upon treatment with zinc revealed different results when compared to the misregulation of transcripts shown through the RNA-sequencing experiment.

One of the hypotheses surrounding Cav3's role in NTC, is the idea that it is acting as mechanical developmental checkpoint, detecting the completion of NTC, and signaling through calcium to move on to the next developmental process. I thus sought to manually perturb the process. Although efforts to produce quality *in situs* of Cav3 have been largely unsuccessful, it does appear that Cav3 is expressed in a few cells in the mid-hindbrain region of the embryo. Since the closing of the neural tube occurs in a zipper-like manner from the

posterior to the anterior end, perhaps disrupting the progression manually around where Cav3 expression is seen could also reproduce the open brain phenotype. Bisection of the embryos using a fine wire anteriorly to the closing zipper was quite effective in producing the desired phenotype. However, transcriptional analyses suggest that the downstream signaling was not affected in these bisected embryos in the same manner as *bugeye* mutants. While it may not provide further insight into the role of Cav3 in NTC, it is certainly an interesting result of manual disruption worth further investigation.

## B. Introduction

A major challenge that comes with working with the *bugeye* mutant is the late onset of the phenotype. It is not until the very late tailbud or hatching stages – well past neurulation – that the open brain phenotype becomes apparent. Despite this, the requirement for Cav3 is between mid-neurula and mid tailbud stages, the time frame in which NTC occurs and the anterior neuropore is fully closed (Abdul-Wajid et al., 2015).

Additionally, homozygous *bugeye* larvae do not properly undergo metamorphosis upon attachment, preventing them from becoming an adult. Due to this, the mutant line must be propagated as heterozygotes and crossing two heterozygotes results in only a quarter of larvae displaying the open brain phenotype. With the added challenge of a late onset phenotype, it has thus far proven impossible for us to identify *bugeye* mutants during neurulation when the

neural tube is closing. This has prohibited extensive investigation of the role of Cav3 as well as downstream targets during NTC.

We wanted to explore the possibility of producing an open brain phenotype through non-genetic means. If there was a way to do so with high efficiency, we could presumably analyze the embryos at an earlier stage with a high level of confidence that the open brain phenotype was present. Here, I will describe three approaches to addressing this problem that also allow us to further investigate the role of Cav3 in the process of NTC.

The simplest way to do so would be to pharmacologically inhibit Cav3. This has been done with the T-type calcium channel blocker, mibefradil. However, despite a reliable production of the open brain larvae with use of this drug, the percentage remains quite low with around 20-25% of the embryos displaying the phenotype. Another prominent inhibitor of T-type $Ca^{2+}$ channels are various divalent cations including zinc ($Zn^{2+}$) (Lacinová, 2011). Zinc has been widely used in cultured cells as a potent inhibitor of Cav3.2 (Huc et al., 2009), which is the channel shown to be required for proper neural tube closure in *Xenopus* (Abdul-Wajid et al., 2015). By utilizing a chemical inhibitor, such as zinc, we may be able to produce embryos in which 100% of them have an open neural tube.

Next, I will describe two additional pharmacological treatments that could produce the same result, but target receptors that may be acting upstream of Cav3 also allowing us to further investigate the function of this channel in NTC.

Further investigation of the *bugeye* mutant in NTC has revealed a host of transcripts that are misregulated due to defects in Cav3 (Smith et al., 2021). We hypothesize that Cav3 may be acting as a mechanical monitor of NTC. Upon proper closure, Cav3 signals to downregulate a host of transcripts necessary for NTC, while the embryo presumably upregulates those necessary for the next developmental processes. In *bugeye* mutants several of these transcripts are abnormally upregulated, perhaps due to inadequate downregulation, resulting in improper sealing of the neural tube, perhaps by persistence of repulsion factors, that results in the open brain phenotype.

In other contexts, stretch-activated mechanosensitive ion channels respond to mechanical stimuli to modulate $Ca^{2+}$ signaling and homeostasis (Du et al., 2020; Qiu et al., 2019). We wanted to investigate whether such channels could be activated in response to the mechanical closing of the neural tube and coupled to Cav3 to mediate the response required for neural fold fusion and sealing. To investigate this, we utilized two trivalent cations that are known to be general blockers of mechanoreceptors: lanthanum ($La^{3+}$) and gadolinium ($Gd^{3+}$) (Ding and Pickard, 1993; Sato et al., 2003; Soga et al., 2004) and analyzed for presence of the open brain phenotype displayed by *bugeye* mutants. While they have been extensively used as a mechanoreceptor blocker, lanthanum has also been shown to be an inhibitor of calcium channels in general (Sato et al., 2003).

The last approach to further investigating the *bugeye* mutant was manual bisection of neurulating embryos. It has been shown that neural tube closure occurs in a zipper like manner from the posterior to the anterior end driven by

sequential activation of junctional myosin (Hashimoto et al., 2015). Although detection of the transcript for *Cav3* by *in situ* hybridization has been difficult, it does appear that it is expressed in a few cells in the mid-hind brain region of the embryo. We wanted to investigate whether mechanical disruption of this zipper, perhaps right around the area of *Cav3* expression, could produce the open brain phenotype shown in *bugeye* larvae and analyze the resulting embryos for evidence of the misregulation that is seen in the *Cav3* mutants.

## C. Methods

### Animals

*Ciona robusta* were either collected from the Santa Barbara Harbor, or were ordered from M-REP (Carlsbad, CA). Adults were maintained in a natural seawater facility. Embryos and larvae were obtained by dissecting gametes from 2-3 adults and culturing them in natural seawater at 18°C. Embryos were dechorionated immediately upon fertilization as described previously (Christiaen et al., 2009).

### Drug Treatments

Zinc chloride ($ZnCl_2$) was used at concentration of 500µM. Lanthanum chloride ($LaCl_3$) and gadolinium chloride ($GdCl_3$) were each used at a concentration of 100µM based on preliminary dosing experiments. Each drug was dissolved in molecular grade water to make a 100X solution. Upon reaching the desired stage of development, embryos were given the drug dissolved in

natural sea water. Once the embryos reached the end of the treatment window, they were removed from the drug with a minimum of four sea water washes in 10cm petri dishes coated in 1% agarose. The embryos were then grown to the larval stage where they were scored for phenotype or collected for RNA.

**RT-PCR**

RNA was extracted from open and closed brain larvae using the NucleoSpin RNA XS kit (Macherey-Nagel). Template cDNA was then synthesized from the RNA using the SuperScript IV First-Strand Synthesis System (Invitrogen). RT-PCR was performed with the primers listed in Supplemental Table 2.2 (Chapter 2). Following agarose gel electrophoresis, the results were quantified and analyzed using FIJI (Schindelin et al., 2012).

**Bisections**

Bisecting tools were made by cutting a small piece of fine tungsten wire and feeding it into the end of a glass pasteur pipette tip filled with molten wax. The tungsten wire was sharpened using the flame from a bunsen burner. Embryos were grown to the desired stage and bisected one at a time, carefully separating the anterior portion from the posterior portion in the dish to prevent them from sticking together. Once all the embryos were bisected, the anterior portion were collected and placed in a separate seawater petri dish. Bisected embryos were grown to the larval stage where they were scored or pooled and

collected for RNA. Arrestin staining of larvae was done as described previously (Jiang et al., 2005).

## D. Results

### Pharmacological modulation of T-type $Ca^{2+}$ channels produced an open brain phenotype.

Initial analyses of the treatment of wildtype larvae from mid-neurula to mid tailbud stages with three different pharmacological inhibitors revealed differing degrees of the open brain phenotype. Zinc, a T-type calcium channel inhibitor, produced the largest result with approximately 60% of embryos displaying the OB phenotype (Figure 3.1A). Next, analysis of two mechanoreceptor blockers produced varying results. Treatment with lanthanum gave a slightly lower percentage of embryos with the open brain phenotype than treatment with zinc, whereas gadolinium treatment did not cause the OB phenotype at all (Figure 3.1A). Both zinc and lanthanum show significant levels of the open brain phenotype at much higher levels than are achievable from crossing two heterozygous mutants, however, treatment with lanthanum caused other morphological defects. For example, embryos show a rounded headed with no distinct palps and do not properly elongate in addition to a clear open brain phenotype (Figure 3.1B). Some embryos produced an intermediate open brain phenotype where the pigment spots were on or near the surface of the head and there was a slight protrusion of tissue, but not in a manner characteristic of the

phenotype of *bugeye* mutants (Figure 3.1B’’). Extension of the time window in which the treatment was applied did not significantly improve the percent of open brains (C). Treatment starting at the late gastrula stage did however cause a decrease in viability and resulted in fewer embryos reaching the larval stage. Control embryos displayed a normal morphology (Figure 3.1B’’’). In contrast to lanthanum treatment, embryos treated with zinc displayed the open brain phenotype and no other overtly abnormal morphologies (data not shown). Thus, zinc treatment was chosen to explore further as a candidate for reproducible creation of OB embryos for further study.

RT-PCR was used to analyze the downstream effects of zinc treatment, specifically looking at the group of transcripts shown to be upregulated in *bugeye* larvae (Smith et al., 2021). Zinc treated larvae with open brains were pooled and harvested for RNA and compared to wildtype larvae with closed brains. A subset of the transcripts were slightly upregulated in zinc treated larvae, but others were largely downregulated (Figure 3.1D). This differs quite a bit from the transcriptional profile of *bugeye* mutants (Smith et al., 2021) and suggests that the production of the open brain phenotype may differ mechanistically with zinc treatment.

**Physical perturbation of neurulating embryos produces an open brain phenotype.**

In order to further investigate the hypothesis that Cav3 could be acting as a mechanical monitor of neural tube closure, we wanted to physically inhibit the

progression of the closing zipper and observe whether embryos went on to display the open brain phenotype. To do so, embryos were bisected in front of the closing zipper before, or right at, the mid-neurula stage. This is also near the reported area of Cav3 expression (Abdul-Wajid et al., 2015). These embryos were compared to those bisected at the initial tailbud stage, behind the closing zipper. Following bisection, the anterior portion of the embryos were isolated and allowed to develop to the larval stage. As an additional control, some embryos were left uncut until the larval stage when the heads were isolated for further analysis (bisection scheme showed in Figure 3.2A). The bisected heads were scored for presence or absence of the phenotype and antibody staining for the brain marker arrestin was used to visualize the neural tissue (Figure 3.2B). There was a range of open brain phenotypes observed (Figure 3.3). Some bisected heads displayed morphological defects such as a rounded head or absence of palps (Figure 3.3A-A’’’). Others displayed enlarged and splayed pigment spots (Figure 3.3B-B’’’). There were many embryos showing the open brain phenotype with normal head shape and mature palps, but varying levels of the brain maker arrestin (Figure 3.3C-C’’’).

Overall, manual bisection of embryos at the mid-neurula stage produced a robust open brain phenotype. There were less, but still quite a few, embryos displaying an open brain when cut at the initial tailbud stage behind the closing zipper (Figure 3.4A). When comparing the percentages of open brains, both bisection at the mid-neurula and initial tailbud stages produced the phenotype at

significantly higher levels than control larvae, but bisection at the earlier stage produced significantly more than those bisected at the latter (Figure 3.4B).

Open brain heads from embryos bisected during the mid-neurula stage were pooled and harvested for RNA alongside closed brains from the controls and analyzed by RT-PCR, assaying for the same suite of transcripts upregulated in *bugeye* mutants to determine if physical disruption of the closing zipper, near the area of Cav3 expression, could produce a similar expression profile to that of the mutants. Each of the transcripts analyzed showed a decrease in expression in the bisected open brain embryos (Figure 3.5A). To rule out any changes in transcript expression caused by the act of manual bisection, the open brain heads from mid-neurula bisected embryos were compared to the closed brain heads from initial tailbud bisected embryos. While there was a slight upward trend in expression, this largely did not change the outcome, with most of the genes analyzed still being slightly downregulated compared to controls (Figure 3.5B).

## E. Discussion

The most successful pharmacological treatment in terms of causing the OB phenotype was zinc. More than twice as many embryos display the phenotype compared to crossing two heterozygous *bugeye* mutants with each individual trial producing over 50% open brains and some reaching over 70%. Zinc has been shown to modulate all three vertebrate Cav3s, but it is able to

preferentially inhibit Cav3.2 at much lower concentrations, with an $IC_{50}$ of around 0.8µM (Hazzaz Abouamal et al., 2018; Huc et al., 2009; Lacinová, 2011). However, *Ciona* required a substantially higher $Zn^{2+}$ concentration to produce the open brain phenotype. This could be due to several issues. Given that the Cav3.2 experiments were using cultured mammalian cells, it is possible that there is a difference in how Zn enters the embryo, especially at lower concentrations. Additionally, zinc is strongly hydroscopic and deliquescent substance (Rohe and Wolf, 2000). Upon weighing it out you can readily observe the white salt pulling in water from the atmosphere making it challenging to get a highly precise mass measurement. Interestingly, long term exposure of mammalian cells to $Zn^{2+}$ has also been shown to upregulate T-type calcium channels (Ekstein et al., 2012), indicating the need to be precise in using it as an inhibitor of T-type calcium channels.

Gastrulating embryos may be particularly sensitive to T-type calcium channel inhibitors given the wide range of roles for these channels. This may explain the decrease in viability that occurs when the zinc treatment is started before gastrulation has finished. The optimal time for treatment to result in the OB phenotype appears to be the window during which the neural tube is closing. Despite this, the downstream transcriptional profile of these open brain embryos produced by bisection does not show similar results to that of *bugeye* mutants indicating that the mechanism may vary from that of a Cav3 deficiency.

Utilizing the two mechanoreceptor blockers produced distinct results. Gadolinium produced no evidence of neural tube defects when given

during neurulation, while lanthanum gave a robust open brain phenotype. One pair of ion channels known to mediate mechanosensory responses are the Piezo proteins (Bagriantsev et al., 2014; Du et al., 2020; Reed et al., 2014). Gadolinium has been shown to inhibit mechano-gated channels, including Piezos, but is also reported to have poor selectivity and exerts off-target effects. Piezos are also inhibited by the peptide GsMTx4 (Bae et al., 2011). However, treatment with this peptide did not produce an open brain phenotype in preliminary experiments done on wild-type *Ciona* larvae (data not shown).

While it has been used as a mechanoreceptor blocker, there is evidence that lanthanum is also an inhibitor of calcium channels (Sato et al., 2003). This suggests that the results seen may simply be due to inhibition of Cav3 itself and not from inhibition of mechanoreceptors. Although lanthanum did produce the open brain phenotype, it did so at a reduced level as compared to zinc and caused additional morphological defects in the embryo making it less suitable as an agent to produce OB embryos for studying the mechanisms behind the open brain defect.

Mechanical disruption of neural tube closure by bisection of mid-neurula stage embryos produced a rather robust open brain phenotype at overall percentages slightly higher than even the zinc treatment. The target of bisection at this stage was meant to be just ahead of the closing zipper. Curiously, bisection just behind the closing zipper also gave an open brain phenotype albeit at significantly lower percentages. These embryos are less than 200µm across the anterior-posterior axis, making it difficult to precisely cut. It is possible that

some of the open brains from this group are due to bisection in front of the closing zipper. Additionally, it is possible that the mechanical stress of bisection was able to disrupt zipper progression that had already occurred. Analysis of transcript levels in bisected embryos failed to show similar misregulation to those of *bugeye* mutants, once again suggesting that the physical disruption in neural tube closure differs mechanistically from that of Cav3.

Surprisingly, the open brain phenotype that occurs following bisection is strikingly similar to that of *bugeye* mutants. It is reasonable to think that bisection would have completely disrupted the progress of NTC and resulted in more severe NTDs. Instead, the folds are able to come together enough to produce a largely normal head, but with the brain extruding from the surface. This does provide some credence to the idea that there may be a mechanical monitor for NTC that results in changes to the transcriptional profile of the cells to support the permanent closure of the neural tube. While the mechanisms may not be identical, further studies of the defect produced by bisection may prove fruitful in understanding the basis behind the permanent sealing of the neural folds and closure of the neural tube.

## F. Figures

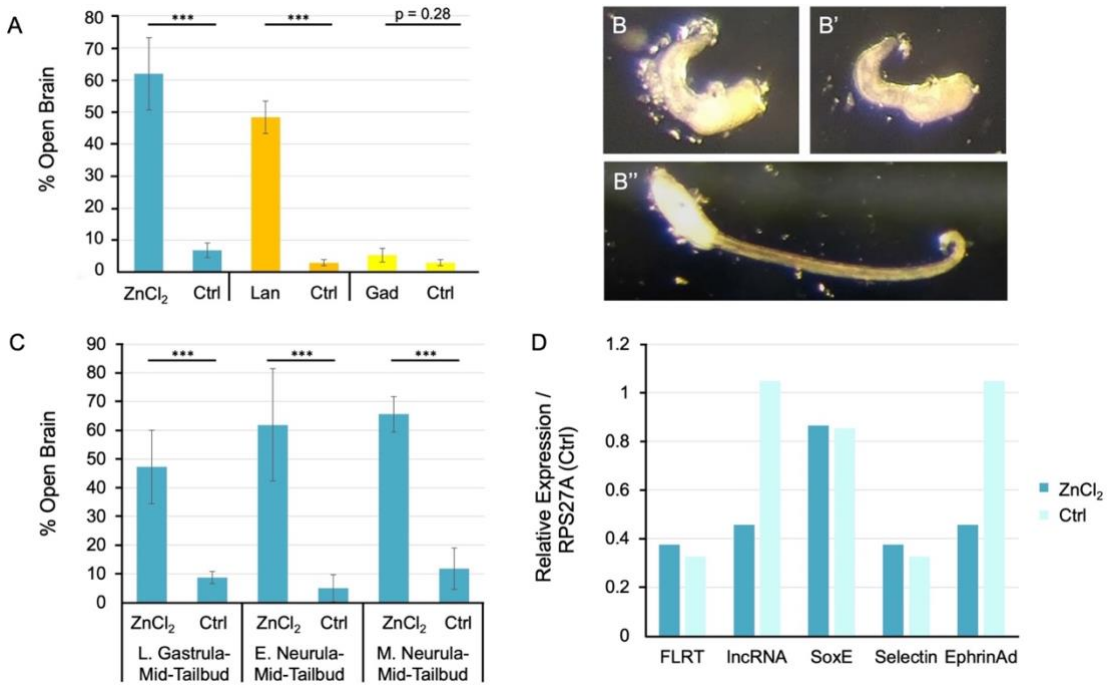


**Figure 3.1. Pharmacological modulation of T-type $Ca^{2+}$ channels produce an open brain phenotype. A**. Larvae scored for open brain phenotype following treatment with 500µm of zinc chloride ($ZnCl_2$), 100µm of lanthanum, or 100µm gadolinium from late gastrula to mid tailbud stages. Drugs were dissolved in water and an equivalent volume of water was used for the controls (Ctrl). **B-B'''.** Larvae imaged upon treatment with lanthanum (B-B'') or control larvae (B'''). B. Open brain phenotype given with lanthanum treatment. B'. Partial open brain phenotype with pigment cells on surface. B'' Control larvae displaying a normal closed brain phenotype. **C**. Larvae scored for open brain phenotype following treatment with 500µm zinc chloride ($ZnCl_2$) during the listed developmental time window. Equivalent volume of water was used as a control. **D**. Analysis of

transcripts known to be upregulated in bugeye mutants in Zn-treated embryos. RT-PCR of open brain embryos following treatment with 500µm zinc chloride ($ZnCl_2$) from late gastrula to mid tailbud stages. ***p < 0.00001, Fisher's exact test.

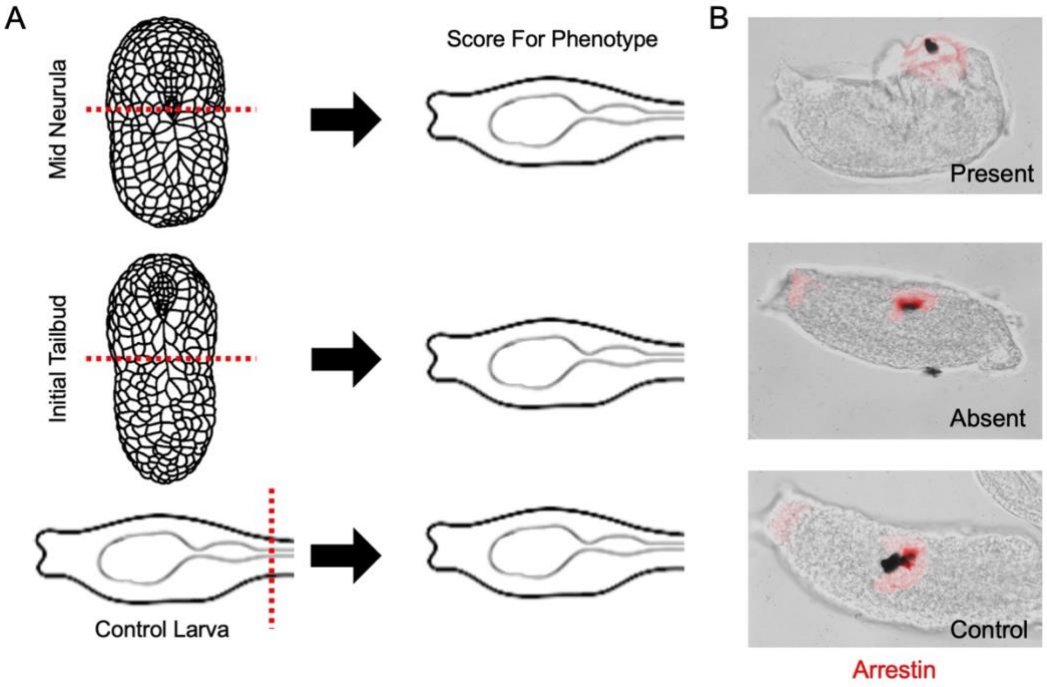


**Figure 3.2. Schematic of bisection protocol and example phenotypes. A**. Diagram showing the stage in which the embryos were cut and then the stage the embryos were grown to and scored for phenotype. **B**. Example phenotypes from each treatment stained with an antibody against arrestin, a brain marker. Top shows an open brain phenotype from bisection at mid-neurula. Middle shows

a closed brain phenotype from bisection at initial tailbud. Bottom shows a control embryo grown until the larval stage.

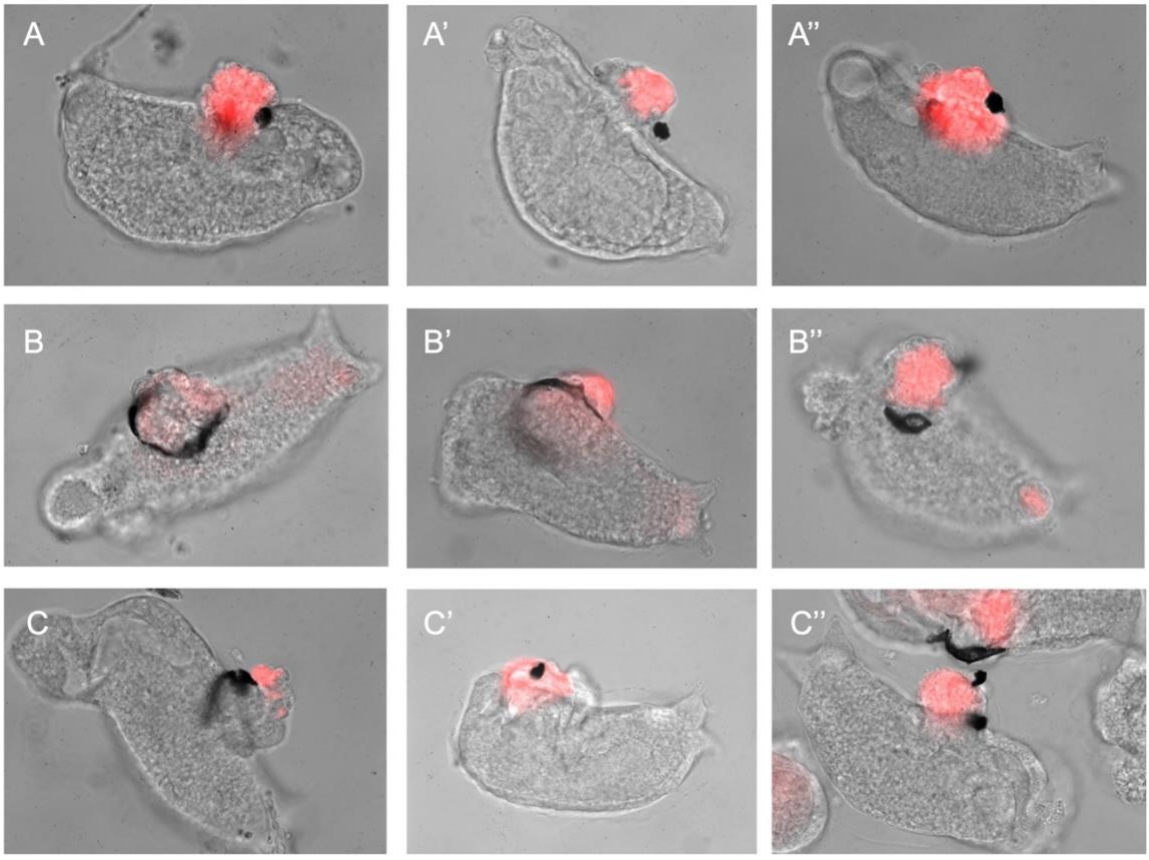


**Figure 3.3. The variety of open brain (OB) phenotypes observed.** Larvae were bisected at the mid-neurula stage as shown in Figure 3.2 and then cultured and scored. **A-A'''**. Larvae display a prominent open brain phenotype with robust arrestin (red) expression but show a rounded head shape and minimal to little evidence of mature palps. **B-B'''**. Larvae display a prominent open brain phenotype with elongated and splayed pigment cells. **C-C'''**. Larvae with an open brain phenotype, largely normal head shape and mature palps. Expression of arrestin was variable with some showing decreased or minimal staining (C). See Figure 3.4 for quantification of phenotypes.

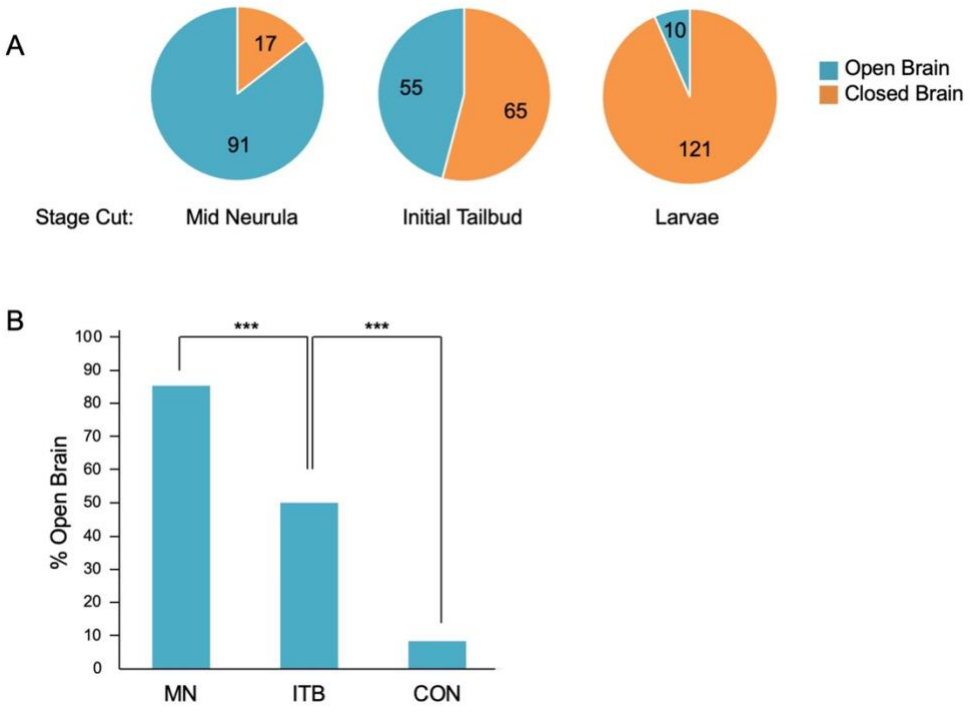


**Figure 3.4. Bisection at mid-neurula and initial tailbud produce an open brain phenotype. A**. Number of embryos from each stage bisected that show an open or closed brain phenotype. **B**. Percentage of open brain phenotype from each stage when bisected. MN = mid-neurula, ITB = initial tailbud, CON = control embryos bisected at the larval stage. ***p < 0.00001, Fisher's exact test.

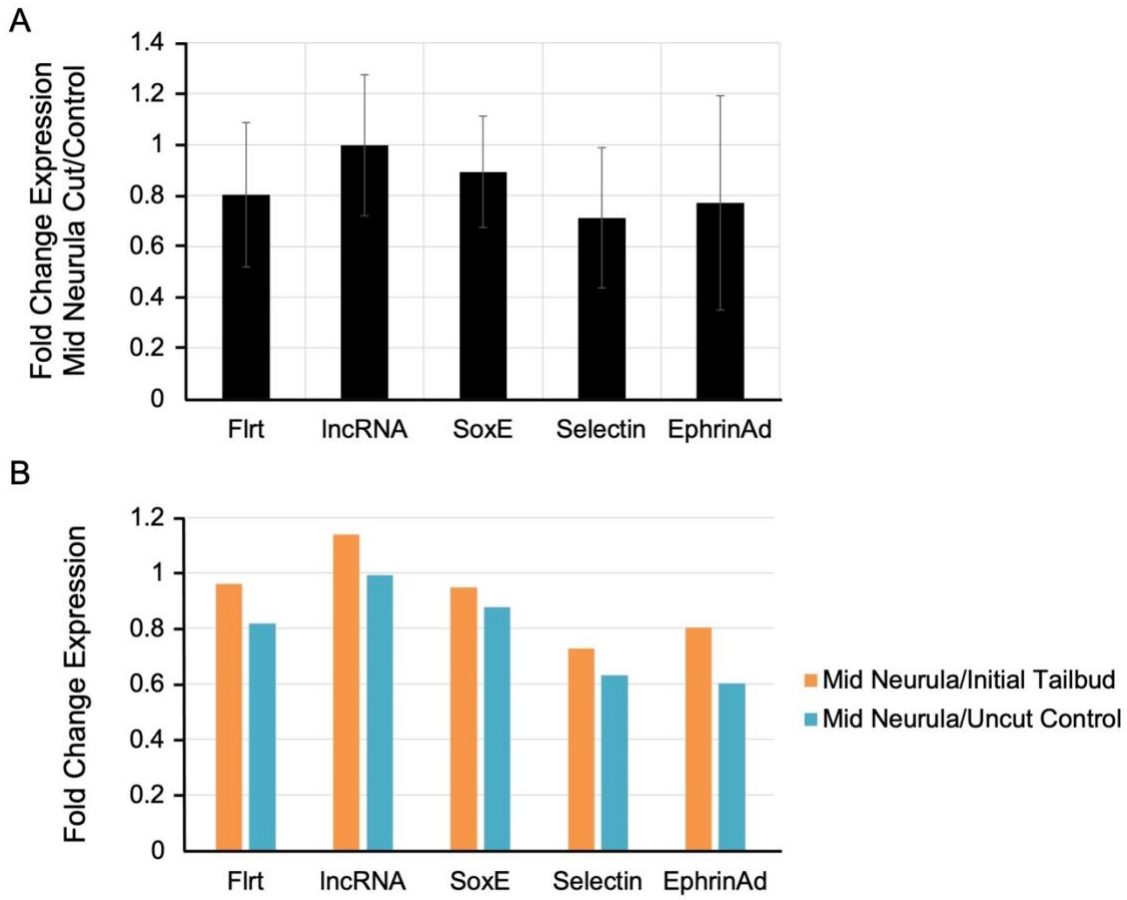


**Figure 3.5. Analysis of the expression of genes misregulated in bugeye mutants in open brain bisected embryos. A**. RT-PCR of indicated transcripts from three separate samples of embryos bisected at the mid-neurula stage. **B**. RT-PCR of open brain larvae collected from mid-neurula bisection of embryos to closed brain larvae collected from either initial tailbud bisection of embryos or uncut control embryos.

## IV. A strategy for analysis of temporally dynamic transcripts to identify genes with novel roles in developmental processes.

### A. Abstract

Expression of several of the genes shown to be downregulated in the *bugeye* mutant show a sharp peak in expression during NTC (Smith et al., 2021). Given this observation we reasoned that other transcripts showing a strong upregulation specifically associated with a distinct developmental stage and/or a sharp decline when that developmental process is completed, such as gastrulation or neurulation, could play a role in that process. Using publicly available RNA-seq datasets to find genes whose expression show this characteristic may reveal novel roles for genes that may have not previously implicated in these developmental processes. A whole embryo RNA-seq dataset was used to identify genes that showed strong upregulation during neurulation. Candidate genes were further narrowed down by associated gene ontology terms, published expression patterns, and possible functions relevant to neural tube closure. This analysis produced several interesting candidates, four of which were targeted for knockout using CRISPR/Cas9. Each of them showed some level of open brain phenotype at significantly higher levels than control embryos. One of particular interest was the *Ciona* gene KH.L169.2 which when compared to the human genome, had similarity to proteins involved in cell adhesion and neurite outgrowth. Using HCR *in situs* to characterize its expression pattern revealed a clear signal in the epidermal tissue surrounding the neural tissue of

the closing neural tube. Further work is needed to determine exactly what role this gene might have in the process but provides proof of concept that this could be a valid way to discover novel roles for genes in a specific developmental process in *Ciona*.

## B. Introduction

Initial analyses of the *Ciona* Cav3 mutant, *bugeye*, revealed aberrant upregulation of *ephrinAd*. In wildtype *Ciona* larva, *ephrinAd* is dramatically down-regulated following neurulation from early through late tailbud stages (Abdul-Wajid et al., 2015). Subsequently, through RNA-sequencing analysis, additional genes were discovered that show a similar upregulation in *bugeye* mutants. Interestingly, both *Flrt* and *Selectin* are not only abnormally upregulated, but show a similar sharp decrease in expression following neurulation in wildtype larvae. This observation led to the hypothesis that genes that show such a significant peak in expression during a discrete developmental period and decline in expression following that period could play a role in the processes that occur in that time frame.

Finding additional genes with similar expression profiles would require transcriptome analysis across several developmental stages and time periods. As with many model organisms, such data are available for *Ciona.* A repository of Ascidian data on Aniseed (aniseed.cnrs.fr), includes graphs showing the expression of individual genes across several developmental time points (Brozovic et al., 2018). For example, there is a clear peak of expression of *Flrt*

during mid-neurula followed by a sharp decrease by the mid tailbud stage, consistent with its potential role in the open brain phenotype of *bugeye* mutants (see Chapter 2). This inspired the idea that already available data could be used to mine for genes with novel roles in specific developmental processes in *Ciona*.

Unsurprisingly, RNA-sequencing has been used in *Ciona* in a variety of ways (Horie et al., 2018; Ilsley et al., 2020; Wei and Dong, 2018) resulting in multiple publicly available datasets that could be used in such an analysis. We chose to utilize the dataset from Aniseed given that we could use the graphical representations of gene expression to find genes with distinct peaks during neurulation, rather than simply genes that decrease following the developmental process. The dataset was from a whole-embryo RNA-sequencing experiment showing expression of transcripts during seven different time points throughout development (Brozovic et al., 2018). Since we already had a NTC mutant, *bugeye*, with a distinct, easy to identify phenotype, we chose to focus on neurulation as an initial analysis to find genes that may play a role in the final stages of closing the neural tube. However, this type of analysis could prove useful for many different developmental stages and processes.

## C. Methods

### Animals

*Ciona robusta* were either collected from the Santa Barbara Harbor, or were ordered from M-REP (Carlsbad, CA). Adults were maintained in a natural seawater facility. Embryos and larvae were obtained by dissecting gametes from 2-3 adults and culturing them in natural seawater at 18°C. Embryos were dechorionated immediately upon fertilization as described previously (Christiaen et al., 2009).

### CRISPR

Electroporations into *C. robusta* were performed as described previously (Veeman et al., 2011; Zeller, 2018). Embryos were dechorionated using 0.1% Trypsin (Sigma T4799) in 10mM TAPS pH 8.2 in filtered sea water as described in (Sardet et al., 2011). Embryos were electroporated with 25µg of each of two sgRNA constructs for each candidate gene. The previously published control sgRNA is a sequence not found in the *Ciona* genome (Stolfi et al., 2014). The sgRNAs were co-electroporated with 32 µg EF1$\alpha$ Cas9 (Stolfi et al., 2014), as well as 15 µg of pBRA>h2bRFP, to serve as a control for electroporation efficiency (Kourakis et al., 2014). Embryos were cultured in 0.2% methylcellulose in filtered sea water on 1% agarose-coated petri dishes at 18°C for 23-25 hours. Hatched larva embryos were anesthetized with 0.04% MS-222 (Sigma) and the neural tube scored as open or closed. CRISPR/Cas9 constructs were generated following the protocol in (Stolfi et al., 2014).

### Hybridization Chain Reaction (HCR) *in situ*

HCR *in situs* were performed as described previously (Kourakis et al., 2019). Briefly, *Ciona robusta* were fixed in 4% paraformaldehyde at various time points using the published staging guide (Hotta et al., 2007). HCR *in situ* probes for each candidate gene were obtained from Molecular Technologies. Sequences are available from the Aniseed website (aniseed.cnrs.fr) using the KH gene model. The larvae were cleared with Slowfade Gold with DAPI (Invitrogen) and imaged on an Olympus FLUOVIEW FV1000 confocal laser scanning microscope and visualized using Imaris (Bitplane).

### Sequencing Data

Whole embryo sequencing data came from an experiment characterizing the expression of genes in *Ciona robusta* across seven stages of embryonic development. Data can be accessed on Aniseed, a repository for ascidian data (Brozovic et al., 2018). Single-cell sequencing data was obtained from experiment published in *Nature* by Cao et al, 2019.

## D. Results

The initial analysis yielded over 700 genes that are downregulated from the neurula stages to the tailbud stages. This list was sorted by degree of downregulation and the top 100 were selected for further analysis. Each gene

was examined on Aniseed (Brozovic et al., 2018) where expression of each gene over time can be visualized. Genes that showed a peak in expression during neurulation, rather than just a downregulation following the process, were selected for further analysis. From this list, genes were excluded or selected based the following criteria. If available *in situ* data showed expression outside of the closing neural tube or surrounding epidermis they were excluded. Genes showing expression in the neural tube were selected for further analysis. Genes without available *in situs* were neither excluded nor selected based on this criterion. Additionally, the top hits resulting from a BLAST search of each gene's protein sequence were analyzed for any known functions that could be relevant to the process of neural tube closure.

This narrowed this list down to 12 genes of interest, four of which were selected for further analysis (Table 4.1). All of these genes were among those with the highest fold change in expression, peaking at mid-neurulation. Three of these genes had top hits from a BLAST search to genes that are known to have a role in neurite outgrowth or synapse development (KH.C10.74, KH.L169.2, KH.C8.605). This was of particular interest given the fact that *Flrt,* a transcript shown to be downregulated in *bugeye* mutants from the RNA-seq analysis, and whose overexpression or knockout recapitulate the phenotype of those mutants, is also known to have a role in synaptogenesis along with its binding partner Latrophilin (Lphn) (Lu et al., 2015; O'Sullivan et al., 2012). One of those genes, KH.L169.2, had orthologous homology to genes known to be involved in cell

adhesion. A fourth gene, KH.C2.957, had orthologous homology to genes involved in craniofacial morphogenesis possibly relating to neural crest cells.

Each of the four candidate genes were individually targeted for knockout by CRISPR/Cas9. Single guide RNAs (sgRNA) were made for each of these four genes with the ubiquitous U6 promoter allowing early expression (Pickett and Zeller, 2018; Sasaki et al., 2014; Stolfi et al., 2014). They were electroporated into one-cell stage embryos along with *Cas9*, expressed under the ubiquitous *Ef1α* promoter (Sasakura et al., 2009; Stolfi et al., 2014). Once the embryos reached the larval stage, they were scored for the open brain phenotype. CRISPR/Cas9 targeted to all four of these genes showed a significantly higher percentage of open brain phenotype than control embryos (Figure 4.1), which displayed some background level of the open brain phenotype.

The localization of expression of the four genes were examined more closely. One, KH2012:KH.C2.957 was already known to be expressed in the neural plate amongst other tissues (Waki et al., 2015). The remaining three (KH.C10.74, KH.L169.2, KH.C8.605) were analyzed for their expression patterns during neurulation using HCR *in situ* analysis (Figure 4.2). Expression patterns for two of the genes were unclear. For KH.C10.74, the *in situ* results were inconsistent and had a high background, making them difficult to interpret. While there appeared to be some expression in the cells in the center of the neural tube, additional replicates failed to provide conclusive evidence for this. The *in situ* analysis of KH.C8.605 was barely detectable. It is possible that this gene has low expression (though detectable by transcriptomic analysis and rtPCR), is

labile, or that there was an issue with the probes. For the third gene, KH.L169.2, a clear pattern of expression was visible in the epidermal tissue surrounding the neural tube. Given the close association between the epidermal and neural tissue that occurs during neurulation, this is a highly interesting result worth further investigation.

## E. Discussion

Over the past several decades our knowledge of the underlying mechanisms controlling developmental processes has greatly increased. Nevertheless, it seems as though answering one question only serves to produce several more. Concurrently, technological advances have made it easier to move from studying the role of individual genes to producing rich datasets that allow us to get a more comprehensive, global picture of how individual processes, like neural tube closure, work in an organism. It is clear that there are still gaps in our knowledge of that process, given that neural tube defects remain some of the most prevalent birth defects occurring today (Avagliano et al., 2019). However, by taking advantage of much of the data that already exists, including these large datasets, it is possible that we can glean insights into the missing pieces of the puzzle.

This brief analysis utilized publicly available RNA-seq data to identify genes whose expression is largely restricted to periods of time in which specific developmental processes occurred. It resulted in the discovery of four additional genes that appear to have a role in NTC in *Ciona.* When these genes are

individually knocked out via CRISPR, produced a phenotype similar to that of *bugeye* mutants. Additionally, are orthologs to genes known to have roles in neurite outgrowth. With further research this may lead to more support for the idea that mechanisms controlling neurite outgrowth may be acting in a similar role during the final stages of closing the neural tube. One candidate in particular, KH.L169.2, shows an interesting expression pattern in the epidermal tissue surrounding the neural tube. A BLAST search of the protein product of this gene against the human genome gives a top hit to a heparan sulfate proteoglycan. This protein is component of basement membranes and is involved with many biological activities (Yamashita et al., 2018). Null mice for this gene show both severe heart and brain defects and die around embryonic day 10-12 (Martinez et al., 2018). Among other defects these mice display a phenotype consistent with exencephaly (Arikawa-Hirasawa et al., 1999). As observed in our *in situ* analysis, it shows no expression in the central nervous system of mice during embryogenesis (Handler et al., 1997). Studies have reported that the integrity of the overlying ectodermal layer that normally would encompass the brain is compromised in these null mice leaving behind small open clefts about 20-30μm in size (Costell et al., 1999). As described previously, the final stages of NTC involve a complex exchanging of cell-cell junctions involving both neural and epidermal tissue. Therefore, the expression of this gene, that when knocked out causes NTC failure, in the cells immediately adjacent to the neural tissue of the closing neural tube could play a role in such a process. This would of course

need to be validated with further experimentation but provides proof of concept that such an analysis could be useful in learning more about the underlying mechanisms of the final stages of NTC in *Ciona*.

Here we have focused on a single RNA-seq dataset looking at expression profiles of whole embryos over time, however the advancement of technology has made it capable to analyze transcriptomics on the single-cell level (Stuart and Satija, 2019). We utilized a second dataset in which single-cell sequencing data was obtained from an experiment profiling the expression of over 90,000 cells isolated from *Ciona intestinalis* at ten different developmental stages beginning with gastrulation all the way up through the larval stage (Cao et al., 2019). These data were analyzed for genes that are not only specifically downregulated following neurulation, but also enriched for neural tissue. Using similar strategies as those employed for the whole embryo dataset, the total list of downregulated genes in neural tissue was narrowed down to a smaller list of 46 potential candidate genes (Supplemental Table 4.1) providing abundant fodder for continued exploration.

This type of analysis could extend to other developmental processes and even other organisms but will be limited by the data available. Different types of data could prove beneficial over others depending on what is being studied. In this situation, we were able to utilize a whole embryo RNA-seq dataset. It is important to note that the simplicity of *Ciona* makes it much more amenable to such an analysis and that a similar one in a more complex, higher order organism would most likely not yield the same results. Single cell sequencing

data could prove informative for certain studies, allowing for analysis of genes showing a peak of expression in a specific tissue type and may be more informative than whole embryo data in a larger and more complex organism.

The abundance of data generated in these studies speaks to the rapid development of technology. Finding creative ways to analyze this already existing data may help to glean new insights into these processes. This can begin to fill in some of the gaps in our knowledge and can serve as a jumping off point for further investigation.

## F. Figures & Tables

**Table 4.1**. Top candidate genes from analysis of whole embryo RNA-sequencing data showing a distinct decrease in expression from the neurula stages to the early tailbud stages. Genes are listed in descending order based on the log fold change in expression. Candidates were selected from the initial list of over 700 genes and selected for those whose overall peak expression was during neurulation. They were furthered screened for gene ontology (GO) terms, available expression patterns, and potential functional relevance to neural tube closure. Bold font indicates genes that were selected for further analysis.

| Ciona Gene Identifier | logFC | Best Human Hits (BLAST) |
|---|---|---|
| **KH2012:KH.C10.74** | **-4.956** | **ADORA1, ADORA2A/B** |
| KH2012:KH.C1.1016 | -2.255 | NR5A1, NR6A1, RXRG |
| **KH2012:KH.C2.957** | **-2.009** | **DLX1, MSX1, MSX2** |
| **KH2012:KH.L169.2** | **-1.995** | **HSPG2, VCAM1, IGSF9B** |
| KH2012:KH.C5.580 | -1.806 | FUT8, SH3KBP1 |
| **KH2012:KH.C8.605** | **-1.671** | **MUSK, ROR1, ROR2** |
| KH2012:KH.C4.366 | -1.213 | ERF, ETV3, ETV3L |
| KH2012:KH.C9.53 | -1.105 | ARMC4, CTNNB1, JUP |
| KH2012:KH.C7.107 | -1.057 | PTPN1, PTPN2, PTPN4 |
| KH2012:KH.C9.717 | -1.047 | FOXF1, FOXH1, FOXQ1 |
| KH2012:KH.C2.899 | -0.978 | BRK1, Q8WUW1 |
| KH2012:KH.C7.167 | -0.947 | LAMC1, LAMC2, LAMC3 |

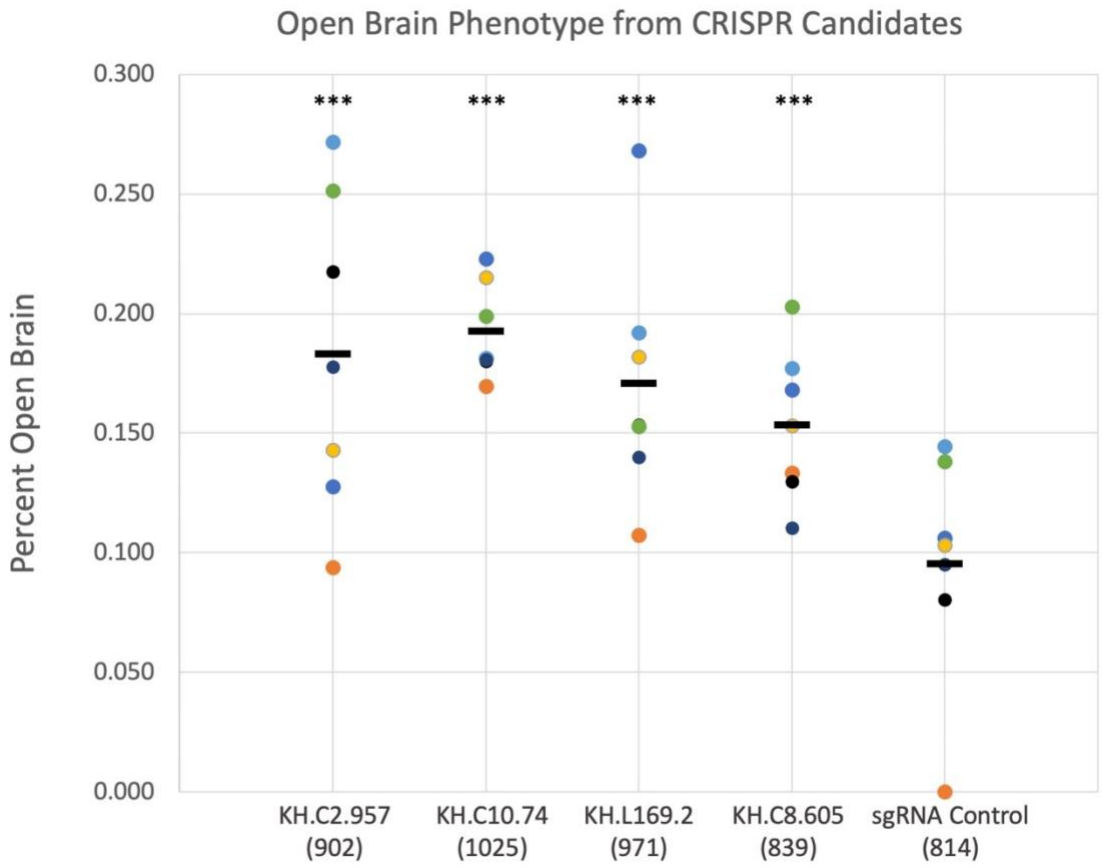


**Figure 4.1**. **CRISPR/Cas9 gene editing of four candidate genes results in an open brain phenotype**. Percent open brain phenotype in wild-type embryos resulting from CRISPR/Cas9 with sgRNAs targeted to the gene indicated. Each dot is an independent replicate. Number of larvae analyzed for each gene is indicated in parentheses below the gene name. ***$p < 0.00001$, Fisher's exact test.

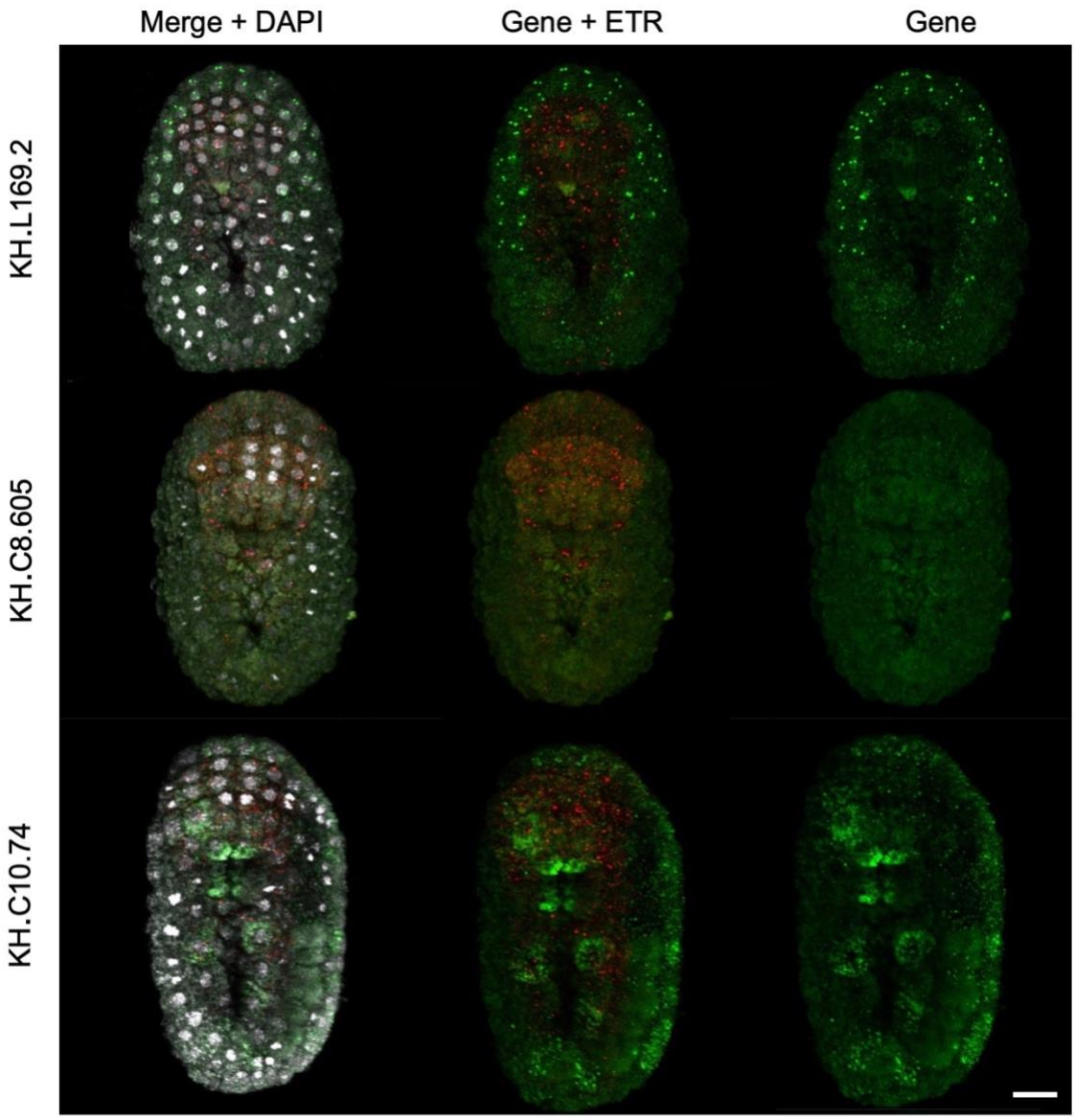


**Figure 4.2**. **Expression of candidate genes by hybridization chain reaction *in situs* of early neurula stage embryos.** Each candidate gene is shown in green (gene identifier specified to the left), the pan-neural marker ETR is red, and nuclei are stained with DAPI are shown as white. Scale bar = 20 µm.

**Supplemental Table 4.1**. Top candidate genes from analysis of single-cell embryo RNA-sequencing data showing a distinct decrease in expression during any two stages from early neurula to initial tailbud. Genes are listed in descending order based on the log fold change in expression.

| Ciona Gene Identifier | logFC | Stage | Best Human Hits |
|---|---|---|---|
| KH2012:KH.C7.269 | -1.028 | earN-latN | no significant similarity found (BLAST) |
| KH2012:KH.C9.234 | -0.947 | earN-latN | no significant similarity found (BLAST) |
| KH2012:KH.S460.5 | -0.923 | earN-latN | SRD5A1/2, TECR |
| KH2012:KH.C14.227 | -0.920 | earN-latN | no significant similarity found (BLAST) |
| KH2012:KH.C6.26 | -0.902 | earN-latN | GJA10/4, GJB1 |
| KH2012:KH.C2.271 | -0.881 | earN-latN | no significant similarity found (BLAST) |
| KH2012:KH.C10.78 | -0.869 | earN-latN | KDELR1/2/3 |
| KH2012:KH.C8.633 | -0.836 | earN-latN | ATP6V0B/C, SLC9A5 |
| KH2012:KH.C3.248 | -0.770 | earN-latN | RPS27/L |
| KH2012:KH.S521.4 | -0.769 | earN-latN | GABARAP/L1/L2 |
| KH2012:KH.C3.174 | -0.768 | earN-latN | no significant similarity found (BLAST) |
| KH2012:KH.C4.224 | -0.756 | earN-latN | ALCAM, BCAM, MCAM |
| KH2012:KH.C11.339 | -0.754 | earN-latN | RPLP2 |
| KH2012:KH.C2.499 | -0.746 | earN-latN | NPC2 |
| KH2012:KH.C6.115 | -0.719 | earN-latN | CGREF1, CHP1, MCFD2 |
| KH2012:KH.C9.717 | -0.715 | earN-latN | FOXF1/H1/Q1 |
| KH2012:KH.L157.5 | -0.703 | earN-latN | ATP1A1/2/3 |
| KH2012:KH.L57.28 | -0.695 | earN-latN | NPBWR1, RGR, RRH |
| KH2012:KH.C1.835 | -0.691 | earN-latN | ERGIC1/2/3 |
| KH2012:KH.C10.31 | -0.685 | earN-latN | ARL6IP5, RABAC1 |
| KH2012:KH.C13.29 | -0.631 | earN-latN | MRPS7, RPS5 |

| | | | |
|---|---|---|---|
| KH2012:KH.S1641.2 | -0.614 | earN-latN | no significant similarity found (BLAST) |
| KH2012:KH.C4.90 | -0.598 | earN-latN | SLC35F1/6 |
| KH2012:KH.C11.271 | -0.587 | latN-iniTI | NDUFAB1 |
| KH2012:KH.L114.13 | -0.581 | earN-latN | LTC4S, MGST2/3 |
| KH2012:KH.L154.31 | -0.565 | earN-latN | ACTA2/B/G1 |
| KH2012:KH.C1.264 | -0.548 | earN-latN | YBX1/2/3 |
| KH2012:KH.L20.54 | -0.532 | earN-latN | RPL39/39L |
| KH2012:KH.C7.264 | -0.515 | earN-latN | RPS12 |
| KH2012:KH.S852.1 | -0.499 | earN-latN | RPS15 |
| KH2012:KH.L10.10 | -0.482 | earN-latN | AC138811.2, RPS15A |
| KH2012:KH.L53.16 | -0.466 | earN-latN | TMED10/4/9 |
| KH2012:KH.L154.5 | -0.449 | earN-latN | HIST2H3A/C/D |
| KH2012:KH.C3.143 | -0.433 | earN-latN | PMM1/2 |
| KH2012:KH.C7.461 | -0.416 | latN-iniTI | COQ3, METTL7B, NDUFAF5 |
| KH2012:KH.C7.365 | -0.400 | latN-iniTI | LSM4, SNRPD1/3 |
| KH2012:KH.C5.25 | -0.383 | latN-iniTI | SLC25A4/5/6 |
| KH2012:KH.C5.15 | -0.367 | latN-iniTI | ATP5MD |
| KH2012:KH.L141.45 | -0.350 | latN-iniTI | no significant similarity found (BLAST) |
| KH2012:KH.C14.553 | -0.334 | latN-iniTI | H2AFV/Z, HIST2H2AC |
| KH2012:KH.C14.4 | -0.317 | latN-iniTI | ADRB2, P2RY12, RGR |
| KH2012:KH.C2.505 | -0.301 | latN-iniTI | C2orf68 |
| KH2012:KH.C8.730 | -0.284 | latN-iniTI | no significant similarity found (BLAST) |
| KH2012:KH.C6.283 | -0.268 | latN-iniTI | AL359922.1, MTAP, PNP |
| KH2012:KH.C1.115 | -0.251 | latN-iniTI | RPS29 |
| KH2012:KH.C4.328 | -0.235 | latN-iniTI | no significant similarity found (BLAST) |

## V. Enduring Questions

Discovery of the *bugeye* mutant has led to some informative analyses on the final stages of NTC in *Ciona* embryos. This is a complex process that is often given little attention in diagrams, textbooks, and discussions of neurulation. There is abundant information on the earlier stages of NTC including neural plate induction, fold formation, and relevant mechanisms such as apical constriction. However, it seems that the complexity of this final junctional exchange has left us with gaps in our knowledge of exactly how this process takes place.

In the literature, there are several processes that are often attributed to controlling this final step. One of them is the migration of neural crest cells from the area connecting the neural epithelium to the non-neural ectoderm effectively separating the two tissues. Many models show these cells migrating from between the neural tube and the epidermis leaving an empty space behind, suggesting they have a major role in the separation of the two tissues (Gilbert, 2000). However, it has long been shown that the migration of neural crest differs in the cranial and spinal region. In the cranial region in chick embryos, the cells detach and migrate well before neural tube closure (Morris-Kay and Tan, 1987), whereas in the spinal region the migration occurs several hours after NTC is complete (Erickson and Weston, 1983). This suggests that it may have a role in the separation, but it is certainly not the only mechanism at play. Even so, other roles for neural crest in NTC, apart from tissue separation, have been described, such as their role in enabling dorsolateral bending of the neural fold edges (Copp, 2005). In *Ciona,* there is evidence for neural crest like cells (Abitua et al.,

2012; Jeffery, 2006), but not along the entirety of the neural plate borders, and no evidence of their role in neural tube closure. Other processes such as the deposition of extracellular matrix between the two tissues and midline spanning cellular protrusions from the neural folds are thought to be important for this process (Martins-Green, 1988; Nikolopoulou et al., 2017). However, it remains unclear exactly what their role is.

The *bugeye* mutant has revealed a novel role for a T-type calcium channel, Cav3, in the process of NTC (Abdul-Wajid et al., 2015). We have shown (Chapter 2, Smith et al., 2021) that there is a suite of abnormally upregulated transcripts resulting from defects in Cav3 that are implicated in the proper closure of the neural tube. Despite this, numerous questions remain. The first is exactly how Cav3 is acting during neural tube closure. We have yet to elucidate the mechanism of action from Cav3 to misregulation of these cell adhesion molecules. Our hypothesis remains that Cav3 is acting as a monitor of neural tube closure, signaling to the cell to down regulate transcripts required for neural tube closure and that this down-regulation may result in the elimination of a repulsive signal that would otherwise interfere with the sealing of the neural tube.

Manual disruption of the closing zipper during NTC in *Ciona* causes embryos to display an open-brain phenotype similar to that of *bugeye* mutants. This is consistent with a model whereby Cav3 is a mechanical monitor of NTC that is required for expression of proper adhesion cues and proteins. We suspected that perhaps stretch-induced mechanoreceptors could be mediating this response. However, use of a broad mechanoreceptor blocker, gadolinium

($Gd^{3+}$) failed to produce the open brain phenotype. Another mechanoreceptor blocker, lanthanum ($La^{3+}$) did produce the phenotype, but $La^{3+}$ has also been shown to block calcium channels and given the results of the two inhibitors it is likely that its effects are due to blocking Cav3 rather than a specific mechanoreceptor (Chapter 3). Further analysis of the molecular and cellular mechanisms underlying the open brain phenotype may help us to identify other players in this process. Live imaging of embryos following bisection could prove an informative next step in this investigation.

Another remaining question is the mechanism behind Flrt's control of neural tube closure. Flrt has been most extensively studied in the context of neurite outgrowth and synapse development through interacting with Lphn to either promote outgrowth and development, or to discourage it (Lu et al., 2015; O'Sullivan et al., 2012). Flrt and Lphn are both expressed in the closing neural tube in opposing domains. Curiously, both Flrt and Lphn have a dynamic expression pattern in the closing neural tube as closure progresses. This suggests that they are not acting as long-term stabilizing molecules, but rather play a transient role in neural tube sealing. Analysis of the localization of Flrt protein in the neural tube could give further indication of where and when it is acting during this process.

Lastly, what is the connection of neurite outgrowth machinery and mechanisms to neural tube closure? Both positive (attractive) and negative (repulsive) cues are using to guide a growing neurite ensuring that the proper connections are made. This process is mediated by many different cell adhesion

molecules such as NCAM and N-cadherin (Kiryushko et al., 2004). ACAM, an ascidian cell adhesion molecule related to NCAM, has also been shown to have a role in NTC in *Ciona* (Morales Diaz et al., 2016). We have shown here that both NCAM and ACAM knockout lead to open brain phenotypes (Chapter 2). Our analyses have also demonstrated that additional proteins involved in neurite outgrowth are implicated in the closing of the neural tube, including both Flrt and Lphn. Interestingly, T-type calcium channels may also be tied to this process with reported roles in axonal and dendritic outgrowth. For example, using chick embryo motor neurons, it was shown that highly localized $Ca^{2+}$ oscillations are originated from these channels and are necessary for the expression of guidance molecules in the migrating axons of the neurons. (Wang et al., 2009; Weiss and Zamponi, 2019). Further investigation into these processes that control neurite outgrowth may reveal shared mechanisms in NTC. It is possible that positive cues involved in this process could mediate the connection of the neuroepithelial cells and/or the non-neural ectoderm cells across the neural folds promoting adhesion. Conversely, repulsive signals between the two tissue types could mediate the release of those cell-cell junctions that are necessary for proper closure of the neural tube.

Overall, the *bugeye* mutant has allowed for identification of additional effectors involved in neural tube closure. The simplicity of the basal chordate body plan in *Ciona* makes it an attractive and relevant model for further investigating the underlying mechanisms of NTC. Further studies of both the *bugeye* mutant and NTC in *Ciona* can help to fill in gaps in our knowledge of how

such a crucial morphogenetic process is accomplished and should provide insight into human neural tube birth defects and their prevention.

## VI. References


Abdul-Aziz, N.M., Turmaine, M., Greene, N.D.E., and Copp, A.J. (2009). EphrinA-EphA receptor interactions in mouse spinal neurulation: implications for neural fold fusion. Int. J. Dev. Biol. *53*, 559–568.

Abdul-Wajid, S., Veeman, M.T., Chiba, S., Turner, T.L., and Smith, W.C. (2014). Exploiting the extraordinary genetic polymorphism of ciona for developmental genetics with whole genome sequencing. Genetics *197*, 49–59.

Abdul-Wajid, S., Morales-Diaz, H., Khairallah, S.M., and Smith, W.C. (2015). T-type Calcium Channel Regulation of Neural Tube Closure and EphrinA/EPHA Expression. Cell Rep. *13*, 829–839.

Abitua, P.B., Wagner, E., Navarrete, I.A., and Levine, M. (2012). Identification of a rudimentary neural crest in a non-vertebrate chordate. Nature *492*, 104.

Anderson, D., Mehaffey, W.H., Iftinca, M., Rehak, R., Engbers, J.D.T., Hameed, S., Zamponi, G.W., and Turner, R.W. (2010). Regulation of neuronal activity by Cav3-Kv4 channel signaling complexes. Nat. Neurosci. *13*, 333–337.

Anderson, M.J., Schimmang, T., and Lewandoski, M. (2016). An FGF3-BMP Signaling Axis Regulates Caudal Neural Tube Closure, Neural Crest Specification and Anterior-Posterior Axis Extension. PLoS Genet. *12*.

Arikawa-Hirasawa, E., Watanabe, H., Takami, H., Hassell, J.R., and Yamada, Y. (1999). Perlecan is essential for cartilage and cephalic development. Nat. Genet. *23*, 354–358.

Arvanitis, D., and Davy, A. (2008). Eph/ephrin signaling: networks. Genes Dev. *22*, 416–429.

Asmara, H., Micu, I., Rizwan, A.P., Sahu, G., Simms, B.A., Zhang, F.-X., Engbers, J.D.T., Stys, P.K., Zamponi, G.W., and Turner, R.W. (2017). A T-type channel-calmodulin complex triggers αCaMKII activation. Mol. Brain *10*, 37.

Auger, H., Lamy, C., Haeussler, M., Khoueiry, P., Lemaire, P., and Joly, J.-S. (2009). Similar regulatory logic in Ciona intestinalis for two Wnt pathway modulators, ROR and SFRP-1/5. Dev. Biol. *329*, 364–373.

Avagliano, L., Massa, V., George, T.M., Qureshy, S., Bulfamante, G.P., and Finnell, R.H. (2019). Overview on neural tube defects: From development to physical characteristics. Birth Defects Res. *111*, 1455–1467.

Bae, C., Sachs, F., and Gottlieb, P.A. (2011). The Mechanosensitive Ion Channel Piezo1 Is Inhibited by the Peptide GsMTx4. Biochemistry *50*, 6295–6300.

Bagriantsev, S.N., Gracheva, E.O., and Gallagher, P.G. (2014). Piezo proteins: regulators of mechanosensation and other cellular processes. J. Biol. Chem. *289*, 31673–31681.

Bostwick, M., Smith, E.L., Borba, C., Newman-Smith, E., Guleria, I., Kourakis, M.J., and Smith, W.C. (2020). Antagonistic Inhibitory Circuits Integrate Visual and Gravitactic Behaviors. Curr. Biol. CB *30*, 600-609.e2.

Bronner-Fraser, M., Wolf, J.J., and Murray, B.A. (1992). Effects of antibodies against N-cadherin and N-CAM on the cranial neural crest and neural tube. Dev. Biol. *153*, 291–301.

Brozovic, M., Dantec, C., Dardaillon, J., Dauga, D., Faure, E., Gineste, M., Louis, A., Naville, M., Nitta, K.R., Piette, J., et al. (2018). ANISEED 2017: extending the integrated ascidian database to the exploration and evolutionary comparison of genome-scale datasets. Nucleic Acids Res. *46*, D718–D725.

Cao, C., Lemaire, L.A., Wang, W., Yoon, P.H., Choi, Y.A., Parsons, L.R., Matese, J.C., Wang, W., Levine, M., and Chen, K. (2019). Comprehensive single-cell transcriptome lineages of a proto-vertebrate. Nature *571*, 349–354.

Cent. Dis. Control Prev. (1992). Recommendations for the use of folic acid to reduce the number of cases of spina bifida and other neural tube defects. MMWR Recomm. Rep. Morb. Mortal. Wkly. Rep. Recomm. Rep. *41*, 1–7.

Chin, M.-L., and Mlodzik, M. (2013). Drosophila Furrowed/Selectin is a homophilic cell adhesion molecule stabilizing Frizzled and intercellular interactions during PCP establishment. Dev. Cell *26*, 455–468.

Choi, H.M.T., Schwarzkopf, M., Fornace, M.E., Acharya, A., Artavanis, G., Stegmaier, J., Cunha, A., and Pierce, N.A. (2018). Third-generation in situ hybridization chain reaction: multiplexed, quantitative, sensitive, versatile, robust. Development *145*.

Christiaen, L., Wagner, E., Shi, W., and Levine, M. (2009). Electroporation of transgenic DNAs in the sea squirt Ciona. Cold Spring Harb. Protoc. *2009*, pdb prot5345.

Cole, A.G., and Meinertzhagen, I.A. (2004). The central nervous system of the ascidian larva: mitotic history of cells forming the neural tube in late embryonic Ciona intestinalis. Dev. Biol. *271*, 239–262.

Concordet, J.-P., and Haeussler, M. (2018). CRISPOR: intuitive guide selection for CRISPR/Cas9 genome editing experiments and screens. Nucleic Acids Res. *46*, W242–W245.

Conklin, E.G. (1905). The Organization and Cell-lineage of the Ascidian Egg (Academy of Natural Sciences).

Copp, A.J. (2005). Neurulation in the cranial region – normal and abnormal. J. Anat. *207*, 623–635.

Copp, A.J., Greene, N.D.E., and Murdoch, J.N. (2003). The genetic basis of mammalian neurulation. Nat. Rev. Genet. *4*, 784.

Copp, A.J., Stanier, P., and Greene, N.D.E. (2013). Neural tube defects: recent advances, unsolved questions, and controversies. Lancet Neurol. *12*, 799–810.

Costell, M., Gustafsson, E., Aszódi, A., Mörgelin, M., Bloch, W., Hunziker, E., Addicks, K., Timpl, R., and Fässler, R. (1999). Perlecan maintains the integrity of cartilage and some basement membranes. J. Cell Biol. *147*, 1109–1122.

Czeizel, A.E., and Dudás, I. (1992). Prevention of the first occurrence of neural-tube defects by periconceptional vitamin supplementation. N. Engl. J. Med. *327*, 1832–1835.

Dardaillon, J., Dauga, D., Simion, P., Faure, E., Onuma, T.A., DeBiasse, M.B., Louis, A., Nitta, K.R., Naville, M., Besnardeau, L., et al. (2020). ANISEED 2019: 4D exploration of genetic data for an extended range of tunicates. Nucleic Acids Res. *48*, D668–D675.

Davidson, L.A., and Keller, R.E. (1999). Neural tube closure in Xenopus laevis involves medial migration, directed protrusive activity, cell intercalation and convergent extension. Development *126*, 4547–4556.

Deak, K.L., Boyles, A.L., Etchevers, H.C., Melvin, E.C., Siegel, D.G., Graham, F.L., Slifer, S.H., Enterline, D.S., George, T.M., Vekemans, M., et al. (2005). SNPs in the neural cell adhesion molecule 1 gene (NCAM1) may be associated with human neural tube defects. Hum. Genet. *117*, 133–142.

Dehal, P., Satou, Y., Campbell, R.K., Chapman, J., Degnan, B., De Tomaso, A., Davidson, B., Di Gregorio, A., Gelpke, M., Goodstein, D.M., et al. (2002). The draft genome of Ciona intestinalis: insights into chordate and vertebrate origins. Science *298*, 2157–2167.

Delsuc, F., Brinkmann, H., Chourrout, D., and Philippe, H. (2006). Tunicates and not cephalochordates are the closest living relatives of vertebrates. Nature *439*, 965–968.

Ding, J.P., and Pickard, B.G. (1993). Mechanosensory calcium-selective cation channels in epidermal cells. Plant J. *3*, 83–110.

Dobin, A., Davis, C.A., Schlesinger, F., Drenkow, J., Zaleski, C., Jha, S., Batut, P., Chaisson, M., and Gingeras, T.R. (2013). STAR: ultrafast universal RNA-seq aligner. Bioinformatics *29*, 15–21.

Du, G., Li, L., Zhang, X., Liu, J., Hao, J., Zhu, J., Wu, H., Chen, W., and Zhang, Q. (2020). Roles of TRPV4 and piezo channels in stretch-evoked Ca2+ response in chondrocytes. Exp. Biol. Med. Maywood NJ *245*, 180–189.

Ekstein, D., Benninger, F., Daninos, M., Pitsch, J., van Loo, K.M.J., Becker, A.J., and Yaari, Y. (2012). Zinc induces long-term upregulation of T-type calcium current in hippocampal neurons in vivo. J. Physiol. *590*, 5895–5905.

Eom, D.S., Amarnath, S., Fogel, J.L., and Agarwala, S. (2011). Bone morphogenetic proteins regulate neural tube closure by interacting with the apicobasal polarity pathway. Development *138*, 3179–3188.

Erickson, C.A., and Weston, J.A. (1983). An SEM analysis of neural crest migration in the mouse. J. Embryol. Exp. Morphol. *74*, 97–118.

Geelen, J.A.G., and Langman, J. (1977). Closure of the neural tube in the cephalic region of the mouse embryo. Anat. Rec. *189*, 625–639.

Geelen, J.A.G., and Langman, J. (1979). Ultrastructural observations on closure of the neural tube in the mouse. Anat. Embryol. (Berl.) *156*, 73–88.

Gilbert, S.F. (2000). Formation of the Neural Tube. Dev. Biol. 6th Ed.

Gilchrist, M.J., Sobral, D., Khoueiry, P., Daian, F., Laporte, B., Patrushev, I., Matsumoto, J., Dewar, K., Hastings, K.E.M., Satou, Y., et al. (2015). A pipeline for the systematic identification of non-redundant full-ORF cDNAs for polymorphic and evolutionary divergent genomes: Application to the ascidian Ciona intestinalis. Dev. Biol. *404*, 149–163.

Gray, L.S., Schiff, D., and Macdonald, T.L. (2013). A model for the regulation of T-type Ca2+ channels in proliferation: roles in stem cells and cancer. Expert Rev. Anticancer Ther. *13*, 589–595.

Greene, N.D.E., and Copp, A.J. (2014). Neural Tube Defects. Annu. Rev. Neurosci. *37*, 221–242.

Haigo, S.L., Hildebrand, J.D., Harland, R.M., and Wallingford, J.B. (2003). Shroom induces apical constriction and is required for hingepoint formation during neural tube closure. Curr. Biol. CB *13*, 2125–2137.

Handler, M., Yurchenco, P.D., and Iozzo, R.V. (1997). Developmental expression of perlecan during murine embryogenesis. Dev. Dyn. Off. Publ. Am. Assoc. Anat. *210*, 130–145.

Hansen, S.M., Berezin, V., and Bock, E. (2008). Signaling mechanisms of neurite outgrowth induced by the cell adhesion molecules NCAM and N-Cadherin. Cell. Mol. Life Sci. *65*, 3809–3821.

Harrington, M.J., Hong, E., and Brewster, R. (2009). Comparative analysis of neurulation: First impressions do not count. Mol. Reprod. Dev. *76*, 954–965.

Hashimoto, H., Robin, F.B., Sherrard, K.M., and Munro, E.M. (2015). Sequential contraction and exchange of apical junctions drives zippering and neural tube closure in a simple chordate. Dev. Cell *32*, 241–255.

Hazzaz Abouamal, T., Choukairi, Z., and Taoufiq, F. (2018). Functional Exploration Of T-Type Calcium Channels (Cav3.2 And Cav3.3) And Their Sensitivity To Zinc. Open Microbiol. J. *12*, 280–287.

Heisenberg, C.-P., and Bellaïche, Y. (2013). Forces in Tissue Morphogenesis and Patterning. Cell *153*, 948–962.

Holland, P.W.H. (2002). Ciona. Curr. Biol. *12*, R609.

Holmberg, J., Clarke, D.L., and Frisén, J. (2000). Regulation of repulsion versus adhesion by different splice forms of an Eph receptor. Nature *408*, 203–206.

Horie, T., Horie, R., Chen, K., Cao, C., Nakagawa, M., Kusakabe, T.G., Satoh, N., Sasakura, Y., and Levine, M. (2018). Regulatory cocktail for dopaminergic neurons in a protovertebrate identified by whole-embryo single-cell transcriptomics. Genes Dev. *32*, 1297–1302.

Hotta, K., Mitsuhara, K., Takahashi, H., Inaba, K., Oka, K., Gojobori, T., and Ikeo, K. (2007). A web-based interactive developmental table for the ascidian Ciona intestinalis, including 3D real-image embryo reconstructions: I. From fertilized egg to hatching larva. Dev. Dyn. Off. Publ. Am. Assoc. Anat. *236*, 1790–1805.

Huc, S., Monteil, A., Bidaud, I., Barbara, G., Chemin, J., and Lory, P. (2009). Regulation of T-type calcium channels: Signalling pathways and functional implications. Biochim. Biophys. Acta BBA - Mol. Cell Res. *1793*, 947–952.

Hudson, C. (2016). The central nervous system of ascidian larvae. Wiley Interdiscip. Rev. Dev. Biol. *5*, 538–561.

Hudson, C., and Lemaire, P. (2001). Induction of anterior neural fates in the ascidian Ciona intestinalis. Mech. Dev. *100*, 189–203.

Hudson, C., and Yasuo, H. (2005). Patterning across the ascidian neural plate by lateral Nodal signalling sources. Development *132*, 1199–1210.

Hudson, C., Lotito, S., and Yasuo, H. (2007). Sequential and combinatorial inputs from Nodal, Delta2/Notch and FGF/MEK/ERK signalling pathways establish a grid-like organisation of distinct cell identities in the ascidian neural plate. Dev. Camb. Engl. *134*, 3527–3537.

Ilsley, G.R., Suyama, R., Noda, T., Satoh, N., and Luscombe, N.M. (2020). Finding cell-specific expression patterns in the early Ciona embryo with single-cell RNA-seq. Sci. Rep. *10*, 4961.

Imai, K.S., Stolfi, A., Levine, M., and Satou, Y. (2009). Gene regulatory networks underlying the compartmentalization of the Ciona central nervous system. Dev. Camb. Engl. *136*, 285–293.

Isono, K., Nemoto, K., Li, Y., Takada, Y., Suzuki, R., Katsuki, M., Nakagawara, A., and Koseki, H. (2006). Overlapping roles for homeodomain-interacting protein kinases hipk1 and hipk2 in the mediation of cell growth in response to morphogenetic and genotoxic signals. Mol. Cell. Biol. *26*, 2758–2771.

Jackson, V.A., del Toro, D., Carrasquero, M., Roversi, P., Harlos, K., Klein, R., and Seiradake, E. (2015). Structural basis of latrophilin-FLRT interaction. Struct. Lond. Engl. 1993 *23*, 774–781.

Jackson, V.A., Mehmood, S., Chavent, M., Roversi, P., Carrasquero, M., Toro, D. del, Seyit-Bremer, G., Ranaivoson, F.M., Comoletti, D., Sansom, M.S.P., et al. (2016). Super-complexes of adhesion GPCRs and neural guidance receptors. Nat. Commun. *7*, 11184.

Jeffery, W.R. (2006). Ascidian neural crest-like cells: phylogenetic distribution, relationship to larval complexity, and pigment cell fate. J. Exp. Zoolog. B Mol. Dev. Evol. *306B*.

Jiang, D., Munro, E.M., and Smith, W.C. (2005). Ascidian prickle Regulates Both Mediolateral and Anterior-Posterior Cell Polarity of Notochord Cells. Curr. Biol. *15*, 79–85.

Juriloff, D.M., and Harris, M.J. (2012). A consideration of the evidence that genetic defects in planar cell polarity contribute to the etiology of human neural tube defects. Birt. Defects Res. A. Clin. Mol. Teratol. *94*, 824–840.

Jurkovicova-Tarabova, B., Cmarko, L., Rehak, R., Zamponi, G.W., Lacinova, L., and Weiss, N. (2019). Identification of a molecular gating determinant within the carboxy terminal region of Cav3.3 T-type channels. Mol. Brain *12*, 34.

Kasahara, M. (2007). The 2R hypothesis: an update. Curr. Opin. Immunol. *19*, 547–552.

Kim, J., Lei, Y., Guo, J., Kim, S.-E., Wlodarczyk, B.J., Cabrera, R.M., Lin, Y.L., Nilsson, T.K., Zhang, T., Ren, A., et al. (2018). Formate rescues neural tube defects caused by mutations in Slc25a32. Proc. Natl. Acad. Sci. *115*, 4690–4695.

Kiryushko, D., Berezin, V., and Bock, E. (2004). Regulators of Neurite Outgrowth: Role of Cell Adhesion Molecules. Ann. N. Y. Acad. Sci. *1014*, 140–154.

Kourakis, M.J., Reeves, W., Newman-Smith, E., Maury, B., Abdul-Wajid, S., and Smith, W.C. (2014). A one-dimensional model of PCP signaling: polarized cell behavior in the notochord of the ascidian Ciona. Dev. Biol. *395*, 120–130.

Kourakis, M.J., Borba, C., Zhang, A., Newman-Smith, E., Salas, P., Manjunath, B., and Smith, W.C. (2019). Parallel visual circuitry in a basal chordate. ELife *8*, e44753.

Lacinová, L. (2011). T-type calcium channel blockers - new and notable. Gen. Physiol. Biophys. *30*, 403–409.

Lacy, S.E., Bönnemann, C.G., Buzney, E.A., and Kunkel, L.M. (1999). Identification of FLRT1, FLRT2, and FLRT3: a novel family of transmembrane leucine-rich repeat proteins. Genomics *62*, 417–426.

Lemaire, P. (2009). Unfolding a chordate developmental program, one cell at a time: Invariant cell lineages, short-range inductions and evolutionary plasticity in ascidians. Dev. Biol. *332*, 48–60.

Lemaire, P., Smith, W.C., and Nishida, H. (2008). Ascidians and the plasticity of the chordate developmental program. Curr. Biol. CB *18*, R620–R631.

Leresche, N., and Lambert, R.C. (2017). T-type calcium channels in synaptic plasticity. Channels *11*, 121–139.

Lu, Y.C., Nazarko, O.V., Sando, R., Salzman, G.S., Li, N.-S., Südhof, T.C., and Araç, D. (2015). Structural Basis of Latrophilin-FLRT-UNC5 Interaction in Cell Adhesion. Struct. Lond. Engl. 1993 *23*, 1678–1691.

Maretto, S., Müller, P.-S., Aricescu, A.R., Cho, K.W.Y., Bikoff, E.K., and Robertson, E.J. (2008). Ventral closure, headfold fusion and definitive endoderm migration defects in mouse embryos lacking the fibronectin leucine-rich transmembrane protein FLRT3. Dev. Biol. *318*, 184–193.

Martinez, J.R., Dhawan, A., and Farach-Carson, M.C. (2018). Modular Proteoglycan Perlecan/HSPG2: Mutations, Phenotypes, and Functions. Genes *9*, 556.

Martins-Green, M. (1988). Origin of the dorsal surface of the neural tube by progressive delamination of epidermal ectoderm and neuroepithelium:

implications for neurulation and neural tube defects. Dev. Camb. Engl. *103*, 687–706.

Massarwa, R., and Niswander, L. (2013). In toto live imaging of mouse morphogenesis and new insights into neural tube closure. Development *140*, 226–236.

McCarthy, D.J., Chen, Y., and Smyth, G.K. (2012). Differential expression analysis of multifactor RNA-Seq experiments with respect to biological variation. Nucleic Acids Res. *40*, 4288–4297.

McEver, R.P. (2002). Selectins: lectins that initiate cell adhesion under flow. Curr. Opin. Cell Biol. *14*, 581–586.

Morales Diaz, H., Mejares, E., Newman-Smith, E., and Smith, W.C. (2016). ACAM, a novel member of the neural IgCAM family, mediates anterior neural tube closure in a primitive chordate. Dev. Biol. *409*, 288–296.

Morris-Kay, G., and Tan, S.-S. (1987). Mapping cranial neural crest cell migration pathways in mammalian embryos. Trends Genet. *3*, 257–261.

Murdoch, J.N., Doudney, K., Paternotte, C., Copp, A.J., and Stanier, P. (2001). Severe neural tube defects in the loop-tail mouse result from mutation of Lpp1, a novel gene involved in floor plate specification. Hum. Mol. Genet. *10*, 2593–2601.

Nagaoka, T., Kaburagi, Y., Hamaguchi, Y., Hasegawa, M., Takehara, K., Steeber, D.A., Tedder, T.F., and Sato, S. (2000). Delayed Wound Healing in the Absence of Intercellular Adhesion Molecule-1 or L-Selectin Expression. Am. J. Pathol. *157*, 237–247.

Nakashima, K., Yamada, L., Satou, Y., Azuma, J., and Satoh, N. (2004). The evolutionary origin of animal cellulose synthase. Dev. Genes Evol. *214*, 81–88.

Navarrete, I.A., and Levine, M. (2016). Nodal and FGF coordinate ascidian neural tube morphogenesis. Development *143*, 4665–4675.

Nicol, D., and Meinertzhagen, I.A. (1988a). Development of the central nervous system of the larva of the ascidian, Ciona intestinalis L: I. The early lineages of the neural plate. Dev. Biol. *130*, 721–736.

Nicol, D., and Meinertzhagen, I.A. (1988b). Development of the central nervous system of the larva of the ascidian, Ciona intestinalis L: II. Neural plate morphogenesis and cell lineages during neurulation. Dev. Biol. *130*, 737–766.

Nikolopoulou, E., Galea, G.L., Rolo, A., Greene, N.D.E., and Copp, A.J. (2017). Neural tube closure: cellular, molecular and biomechanical mechanisms. Development *144*, 552–566.

Nishida, H. (1987). Cell lineage analysis in ascidian embryos by intracellular injection of a tracer enzyme. III. Up to the tissue restricted stage. Dev. Biol. *121*, 526–541.

Nishimura, T., Honda, H., and Takeichi, M. (2012). Planar Cell Polarity Links Axes of Spatial Dynamics in Neural-Tube Closure. Cell *149*, 1084–1097.

Obican, S.G., Finnell, R.H., Mills, J.L., Shaw, G.M., and Scialli, A.R. (2010). Folic acid in early pregnancy: a public health success story. FASEB J. Off. Publ. Fed. Am. Soc. Exp. Biol. *24*, 4167–4174.

Ogata, S., Morokuma, J., Hayata, T., Kolle, G., Niehrs, C., Ueno, N., and Cho, K.W.Y. (2007). TGF-β signaling-mediated morphogenesis: modulation of cell adhesion via cadherin endocytosis. Genes Dev. *21*, 1817–1831.

Omasits, U., Ahrens, C.H., Müller, S., and Wollscheid, B. (2014). Protter: interactive protein feature visualization and integration with experimental proteomic data. Bioinformatics *30*, 884–886.

O'Sullivan, M.L., de Wit, J., Savas, J.N., Comoletti, D., Otto-Hitt, S., Yates, J.R., and Ghosh, A. (2012). FLRT proteins are endogenous latrophilin ligands and regulate excitatory synapse development. Neuron *73*, 903–910.

Passamaneck Yale J. and Di Gregorio Anna (2005). Ciona intestinalis: Chordate development made simple. Dev. Dyn. *233*, 1–19.

Pertea, M., Kim, D., Pertea, G.M., Leek, J.T., and Salzberg, S.L. (2016). Transcript-level expression analysis of RNA-seq experiments with HISAT, StringTie and Ballgown. Nat. Protoc. *11*, 1650–1667.

Pickett, C.J., and Zeller, R.W. (2018). Efficient genome editing using CRISPR-Cas-mediated homology directed repair in the ascidian Ciona robusta. Genesis *56*, e23260.

Pyrgaki, C., Trainor, P., Hadjantonakis, A.-K., and Niswander, L. (2010). Dynamic imaging of mammalian neural tube closure. Dev. Biol. *344*, 941–947.

Pyrgaki, C., Liu, A., and Niswander, L. (2011). Grainyhead-like 2 regulates neural tube closure and adhesion molecule expression during neural fold fusion. Dev. Biol. *353*, 38–49.

Qiu, Z., Guo, J., Kala, S., Zhu, J., Xian, Q., Qiu, W., Li, G., Zhu, T., Meng, L., Zhang, R., et al. (2019). The Mechanosensitive Ion Channel Piezo1 Significantly Mediates In Vitro Ultrasonic Stimulation of Neurons. IScience *21*, 448–457.

Reed, A., Kohl, P., and Peyronnet, R. (2014). Molecular candidates for cardiac stretch-activated ion channels. Glob. Cardiol. Sci. Pract. *2014*, 9–25.

Robinson, A., Escuin, S., Doudney, K., Vekemans, M., Stevenson, R.E., Greene, N.D.E., Copp, A.J., and Stanier, P. (2012). Mutations in the planar cell polarity genes CELSR1 and SCRIB are associated with the severe neural tube defect craniorachischisis. Hum. Mutat. *33*, 440–447.

Robinson, M., Parsons Perez, M.C., Tébar, L., Palmer, J., Patel, A., Marks, D., Sheasby, A., De Felipe, C., Coffin, R., Livesey, F.J., et al. (2004). FLRT3 is expressed in sensory neurons after peripheral nerve injury and regulates neurite outgrowth. Mol. Cell. Neurosci. *27*, 202–214.

Rohe, D.M.M., and Wolf, H.U. (2000). Zinc Compounds. In Ullmann's Encyclopedia of Industrial Chemistry, (American Cancer Society), p.

Roure, A., Rothbacher, U., Robin, F., Kalmar, E., Ferone, G., Lamy, C., Missero, C., Mueller, F., and Lemaire, P. (2007). A multicassette Gateway vector set for high throughput and comparative analyses in ciona and vertebrate embryos. PLoS One *2*, e916.

Ryan, K., and Meinertzhagen, I.A. (2019). Neuronal identity: the neuron types of a simple chordate sibling, the tadpole larva of Ciona intestinalis. Curr. Opin. Neurobiol. *56*, 47–60.

Salas, P., Vinaithirthan, V., Newman-Smith, E., Kourakis, M.J., and Smith, W.C. (2018). Photoreceptor specialization and the visuomotor repertoire of the primitive chordate Ciona. J. Exp. Biol. *221*.

Sardet, C., Mcdougall, A., Yasuo, H., Chenevert, J., Dumollard, R., Hudson, C., Hebras, C., Le, P.N., and Paix, A. (2011). Embryological Methods in Ascidians: The Villefranche-sur-Mer Protocols.

Sasaki, H., Yoshida, K., Hozumi, A., and Sasakura, Y. (2014). CRISPR/Cas9-mediated gene knockout in the ascidian Ciona intestinalis. Dev. Growth Differ. *56*, 499–510.

Sasakura, Y., Suzuki, M.M., Hozumi, A., Inaba, K., and Satoh, N. (2009). Maternal factor-mediated epigenetic gene silencing in the ascidian Ciona intestinalis. Mol. Genet. Genomics *283*, 99.

Sato, Y., Wada, M., and Kadota, A. (2003). Accumulation response of chloroplasts induced by mechanical stimulation in bryophyte cells. Planta *216*, 772–777.

Satoh, N. (2003). The ascidian tadpole larva: comparative molecular development and genomics. Nat. Rev. Genet. *4*, 285–295.

Satoh, N. (2013). Developmental Genomics of Ascidians (John Wiley & Sons).

Satou, Y., Takatori, N., Yamada, L., Mochizuki, Y., Hamaguchi, M., Ishikawa, H., Chiba, S., Imai, K., Kano, S., Murakami, S.D., et al. (2001). Gene expression profiles in Ciona intestinalis tailbud embryos. Development *128*, 2893–2904.

Schindelin, J., Arganda-Carreras, I., Frise, E., Kaynig, V., Longair, M., Pietzsch, T., Preibisch, S., Rueden, C., Saalfeld, S., Schmid, B., et al. (2012). Fiji: an open-source platform for biological-image analysis. Nat. Methods *9*, 676–682.

Seiradake, E., del Toro, D., Nagel, D., Cop, F., Härtl, R., Ruff, T., Seyit-Bremer, G., Harlos, K., Border, E.C., Acker-Palmer, A., et al. (2014). FLRT Structure: Balancing Repulsion and Cell Adhesion in Cortical and Vascular Development. Neuron *84*, 370–385.

Small, K.S., Brudno, M., Hill, M.M., and Sidow, A. (2007). Extreme genomic variation in a natural population. Proc. Natl. Acad. Sci. U. S. A. *104*, 5698–5703.

Smith, H.M., Khairallah, S.M., Nguyen, A.H., Newman-Smith, E., and Smith, W.C. (2021). Misregulation of cell adhesion molecules in the Ciona neural tube closure mutant bugeye. Dev. Biol. *480*, 14–24.

Soga, K., Wakabayashi, K., Kamisaka, S., and Hoson, T. (2004). Graviperception in growth inhibition of plant shoots under hypergravity conditions produced by centrifugation is independent of that in gravitropism and may involve mechanoreceptors. Planta *218*, 1054–1061.

Stolfi, A., Gandhi, S., Salek, F., and Christiaen, L. (2014). Tissue-specific genome editing in Ciona embryos by CRISPR/Cas9. Development *141*, 4115–4120.

Stuart, T., and Satija, R. (2019). Integrative single-cell analysis. Nat. Rev. Genet. *20*, 257–272.

Suzuki, M., Morita, H., and Ueno, N. (2012). Molecular mechanisms of cell shape changes that contribute to vertebrate neural tube closure. Dev. Growth Differ. *54*, 266–276.

Thiersch, J.B. (1952). Therapeutic abortions with a folic acid antagonist, 4-aminopteroylglutamic acid (4-amino P.G.A) administered by the oral route. Am. J. Obstet. Gynecol. *63*, 1298–1304.

Thiersch, J.B., and Philips, F.S. (1950). Effect of 4-Amino-Pteroylglutamic Acid (Aminopterin) on Early Pregnancy. Proc. Soc. Exp. Biol. Med. *74*, 204–208.

del Toro, D., Carrasquero-Ordaz, M.A., Chu, A., Ruff, T., Shahin, M., Jackson, V.A., Chavent, M., Berbeira-Santana, M., Seyit-Bremer, G., Brignani, S., et al. (2020). Structural Basis of Teneurin-Latrophilin Interaction in Repulsive Guidance of Migrating Neurons. Cell *180*, 323-339.e19.

Veeman, M.T., Newman-Smith, E., El-Nachef, D., and Smith, W.C. (2010). The ascidian mouth opening is derived from the anterior neuropore: Reassessing the mouth/neural tube relationship in chordate evolution. Dev. Biol. *344*, 138–149.

Veeman, M.T., Chiba, S., and Smith, W.C. (2011). Ciona genetics. Methods Mol Biol *770*, 401–422.

Vinson, J.P., Jaffe, D.B., O'Neill, K., Karlsson, E.K., Stange-Thomann, N., Anderson, S., Mesirov, J.P., Satoh, N., Satou, Y., Nusbaum, C., et al. (2005). Assembly of polymorphic genomes: Algorithms and application to Ciona savignyi. Genome Res. *15*, 1127–1135.

Vitko, I., Bidaud, I., Arias, J.M., Mezghrani, A., Lory, P., and Perez-Reyes, E. (2007). The I-II Loop Controls Plasma Membrane Expression and Gating of Cav3.2 T-Type Ca2+ Channels: A Paradigm for Childhood Absence Epilepsy Mutations. J. Neurosci. *27*, 322–330.

Wagner, E., and Levine, M. (2012). FGF signaling establishes the anterior border of the Ciona neural tube. Development *139*, 2351–2359.

Waki, K., Imai, K.S., and Satou, Y. (2015). Genetic pathways for differentiation of the peripheral nervous system in ascidians. Nat. Commun. *6*, 8719.

Wallingford, J.B. (2012). Planar cell polarity and the developmental control of cell behavior in vertebrate embryos. Annu. Rev. Cell Dev. Biol. *28*, 627–653.

Wallingford, J.B., and Harland, R.M. (2001). Xenopus Dishevelled signaling regulates both neural and mesodermal convergent extension: parallel forces elongating the body axis. Development *128*, 2581–2592.

Wallingford, J.B., Niswander, L.A., Shaw, G.M., and Finnell, R.H. (2013). The Continuing Challenge of Understanding, Preventing, and Treating Neural Tube Defects. Science *339*, 1222002.

Wang, S., Polo-Parada, L., and Landmesser, L.T. (2009). Characterization of Rhythmic Ca2+ Transients in Early Embryonic Chick Motoneurons: Ca2+ Sources and Effects of Altered Activation of Transmitter Receptors. J. Neurosci. *29*, 15232–15244.

Wei, J., and Dong, B. (2018). Identification and expression analysis of long noncoding RNAs in embryogenesis and larval metamorphosis of Ciona savignyi. Mar. Genomics *40*, 64–72.

Weiss, N., and Zamponi, G.W. (2019). T-type calcium channels: From molecule to therapeutic opportunities. Int. J. Biochem. Cell Biol. *108*, 34–39.

Weiss, N., Hameed, S., Fernández-Fernández, J.M., Fablet, K., Karmazinova, M., Poillot, C., Proft, J., Chen, L., Bidaud, I., Monteil, A., et al. (2012). A Cav3.2/Syntaxin-1A Signaling Complex Controls T-type Channel Activity and Low-threshold Exocytosis. J. Biol. Chem. *287*, 2810–2818.

Wilde, J.J., Petersen, J.R., and Niswander, L. (2014). Genetic, Epigenetic, and Environmental Contributions to Neural Tube Closure. Annu. Rev. Genet. *48*, 583–611.

Yamagishi, S., Hampel, F., Hata, K., Del Toro, D., Schwark, M., Kvachnina, E., Bastmeyer, M., Yamashita, T., Tarabykin, V., Klein, R., et al. (2011). FLRT2 and FLRT3 act as repulsive guidance cues for Unc5-positive neurons. EMBO J. *30*, 2920–2933.

Yamashita, Y., Nakada, S., Yoshihara, T., Nara, T., Furuya, N., Miida, T., Hattori, N., and Arikawa-Hirasawa, E. (2018). Perlecan, a heparan sulfate proteoglycan, regulates systemic metabolism with dynamic changes in adipose tissue and skeletal muscle. Sci. Rep. *8*, 7766.

Ybot-Gonzalez, P., and Copp, A.J. (1999). Bending of the neural plate during mouse spinal neurulation is independent of actin microfilaments. Dev. Dyn. *215*, 273–283.

Ybot-Gonzalez, P., Savery, D., Gerrelli, D., Signore, M., Mitchell, C.E., Faux, C.H., Greene, N.D.E., and Copp, A.J. (2007). Convergent extension, planar-cell-polarity signalling and initiation of mouse neural tube closure. Dev. Camb. Engl. *134*, 789–799.

Yukami, T., Hasegawa, M., Matsushita, Y., Fujita, T., Matsushita, T., Horikawa, M., Komura, K., Yanaba, K., Hamaguchi, Y., Nagaoka, T., et al. (2007). Endothelial selectins regulate skin wound healing in cooperation with L-selectin and ICAM-1. J. Leukoc. Biol. *82*, 519–531.

Zaganjor, I., Sekkarie, A., Tsang, B.L., Williams, J., Razzaghi, H., Mulinare, J., Sniezek, J.E., Cannon, M.J., and Rosenthal, J. (2016). Describing the Prevalence of Neural Tube Defects Worldwide: A Systematic Literature Review. PloS One *11*, e0151586.

Zeller, R.W. (2018). Electroporation in Ascidians: History, Theory and Protocols. In Transgenic Ascidians, Y. Sasakura, ed. (Singapore: Springer), pp. 37–48.

Zeller, R.W., Weldon, D.S., Pellatiro, M.A., and Cone, A.C. (2006). Optimized green fluorescent protein variants provide improved single cell resolution of transgene expression in ascidian embryos. Dev. Dyn. *235*, 456–467.

Zhang, J., Biczok, R., and Ruschhaupt, M. (2020). ddCt: The ddCt Algorithm for the Analysis of Quantitative Real-Time PCR (qRT-PCR).

Zhang, Y., Jiang, X., Snutch, T.P., and Tao, J. (2013). Modulation of low-voltage-activated T-type Ca2+ channels. Biochim. Biophys. Acta BBA - Biomembr. *1828*, 1550–1559.